Energy-dependent neutrino mixing parameters at oscillation experiments

K. S. Babu,[1] Vedran Brdar,[2,3] André de Gouvêa,[2] and Pedro A. N. Machado[3]
[1]*Department of Physics, Oklahoma State University, Stillwater, Oklahoma 74078, USA*
[2]*Department of Physics and Astronomy, Northwestern University, 2145 Sheridan Road, Evanston, Illinois 60208, USA*
[3]*Theoretical Physics Department, Fermilab, P.O. Box 500, Batavia, Illinois 60510, USA*

(Received 7 September 2021; accepted 20 May 2022; published 10 June 2022)

Neutrino mixing parameters are subject to quantum corrections and hence are scale dependent. This means that the mixing parameters associated with the production and detection of neutrinos need not coincide since these processes are characterized by different energy scales. We show that, in the presence of relatively light new physics, the scale dependence of the mixing parameters can lead to observable consequences in long-baseline neutrino oscillation experiments, such as T2K and NOνA, and in neutrino telescopes like IceCube. We discuss some of the experimental signatures of this scenario, including zero-baseline flavor transitions, new sources of *CP*-invariance violation, and apparent inconsistencies among measurements of mixing angles at different experiments or oscillation channels. Finally, we present simple, ultraviolet-complete models of neutrino masses, which lead to observable running of the neutrino mixing matrix below the weak scale.

DOI: 10.1103/PhysRevD.105.115014

I. INTRODUCTION

The discovery of neutrino oscillations toward the end of the last century [1,2] launched a diverse, worldwide experimental neutrino oscillation program that is expected to continue, at least, well into the next decade with the DUNE [3] and Hyper-Kamiokande [4] projects, currently under construction. It aims at measuring, sometimes with exquisite precision, the neutrino oscillation phenomenon via a variety of oscillation channels, baselines, and experimental conditions. The ultimate goal is to, broadly speaking, test the three-massive-active-neutrinos paradigm that postulates the existence of three neutral leptons with different masses that interact only via the neutral-current and charged-current weak interactions, as prescribed by the Standard Model of particle physics (SM).

While the three-massive-active-neutrinos paradigm provides an excellent fit to virtually all neutrino data,[1] the current data allow for the presence of more new physics in the neutrino sector. Different, well-motivated new-physics scenarios can be probed by the current and next generation of neutrino experiments. These include the existence of new, light neutral-fermion degrees of freedom that mix with the active neutrinos ("sterile neutrinos"), and new neutrino–matter interactions that manifest themselves at the energies of interest via four-fermion operators ("nonstandard interactions"). The latter are usually associated with heavy new physics and are, in general, strongly constrained, in the absence of a fair amount of fine-tuning, by charged-lepton processes [11–15], with some exceptions (see, for example, Refs. [16–19]).

Here, we explore potential new phenomena associated with new, relatively light degrees of freedom that interact almost exclusively with neutrinos. In these scenarios, constraints from the charged-lepton sector are significantly weaker, while other constraints, including those associated with the existence of new, light degrees of freedom in the early Universe, can be avoided. New interactions between neutrinos and new, light particles can impact neutrino experiments in two different ways: (i) the new states can be produced when neutrinos are produced or detected, leading to changes in the kinematics and flavor structure of neutrino scattering (see, for example, [20–25] and references therein) or (ii) quantum corrections associated with the virtual exchange of the new degrees of freedom can modify neutrino production and detection. Here, we concentrate on the latter, which, to the best of our knowledge, has not been explored extensively in the literature.

[1]There are experimental results that do not fit the three-massive-active-neutrinos paradigm, including searches for electron (anti)neutrino appearance at the LSND [5] and MiniBooNE [6–8] experiments, as well as the so-called reactor antineutrino anomaly [9,10]. Explanations to these remain elusive and will not be considered in any detail here.

At the core of the idea is the fact that, once higher-order corrections are included, the parameters that describe neutrino oscillations are energy dependent. This is neither new nor surprising. For example, the renormalization-group (RG) running of neutrino oscillation parameters between the neutrino-mass-generating scale (often assumed to be much higher than the scale of electroweak symmetry breaking) and the weak scale has been the subject of intense investigation in the literature; see, for instance, Refs. [26–33]. The running of mass and mixing parameters is not exclusive to the neutrino sector: quark masses run significantly above the GeV scale and the running of the bottom and the top masses has been directly observed at lepton and hadron colliders [34–39]. The Cabibbo-Kobayashi-Maskawa matrix elements are also expected to run above the weak scale [40]; this running, however, has never been observed. Below the weak scale, these matrix elements can be treated as constant in the absence of light new physics. This is usually a good approximation since new, light degrees of freedom that couple to quarks are strongly constrained.

Different from the quark sector, however, new light degrees of freedom that couple predominantly to neutrinos are not strongly constrained. If these exist, RG-running effects may be relevant in the context of neutrino oscillation experiments. In this paper, we show that neutrino oscillation probabilities are affected through the mismatch between the leptonic mixing matrix evaluated at the scale (or more precisely momentum transfer) corresponding to the neutrino production and the one at which neutrinos are detected. A careful treatment of the oscillation phenomenon, therefore, requires—for a fixed neutrino energy—twice as many relevant mixing angles (production and detection values). The number of CP-odd parameters is also larger. We find that, while running effects are already strongly constrained, they can impact significantly the current and next generation of neutrino oscillation experiments, including T2K and Noνa. Their presence may lead, for example, to apparent inconsistencies between measurements of oscillation parameters between T2K and Noνa and between "accelerator" and "reactor" measurements of oscillation parameters. On the other hand, there are simple new-physics scenarios that lead to significant low-energy running of the oscillation parameters, including some that are related to the origin of nonzero neutrino masses. Hence, these effects are not only possible, in principle, they may be accessible if neutrino masses are a consequence of relatively light, new physics.

This manuscript is organized as follows. In Sec. II, we set the stage by introducing and discussing the general idea. Section III contains a detailed treatment of neutrino oscillation probabilities in the presence of RG-running effects. First, in Sec. III A, we compute the vacuum oscillation probability, in general, and discuss the more familiar, less cumbersome two-flavor case in some detail; in this simplified framework, we discuss the oscillation probabilities in different useful limits including circumstances when the running effects are small and the case in which the oscillation baseline is zero. We discuss the more useful but much more cumbersome three-flavor scenario concentrating on subsets of the parameter space. In Sec. III B, we discuss matter effects, which are relevant for the long-baseline experiments under consideration. For the two-flavor case, exact expressions are given, while the realistic three-flavor case can only be tackled, for all pragmatic purposes, numerically. In Sec. IV, we discuss two concrete models that lead to large RG-running effects. A quantitative study of the consequences of these models is presented in Sec. V. There, we discuss some consequences for T2K and Noνa in light of constraints from short-baseline experiments (Sec. V A). In Sec. V B, we scrutinize the impact on the flavor composition of ultrahigh-energy neutrinos. Finally, we conclude in Sec. VI.

II. RUNNING OF NEUTRINO MIXING PARAMETERS

A simple way to understand that quantum corrections can lead to nontrivial effects in neutrino oscillations is to investigate the charged-current weak interactions in the mass basis for both charged leptons and neutrinos. In more detail,

$$-\mathcal{L} \supset \frac{g}{\sqrt{2}} U_{\alpha i} \bar{\ell}_\alpha \not{W}^- P_L \nu_i + \text{H.c.}, \tag{2.1}$$

where ℓ_α, $\alpha = e, \mu$, and τ, are the charged-lepton fields, ν_i, $i = 1, 2, 3$, are the neutrino fields with well-defined masses m_1, m_2, and m_3, respectively, g is the $SU(2)_L$ gauge coupling, P_L is the left-chiral projection operator, and $U_{\alpha i}$ are the elements of the leptonic mixing matrix. The product $(gU_{\alpha i})$ can be interpreted as the coupling between a W boson, a charged lepton ℓ_α, and a neutrino ν_i. Once higher-order quantum effects are included, the question of interest here is whether these allow $(gU_{\alpha i})$ to change relative to one another. When this happens, as we discuss carefully below, we can say that the mixing-matrix "runs."

It is easy to see that, ignoring fermion Yukawa coupling effects, higher-order electroweak corrections to $(gU_{\alpha i})$ are trivially proportional to $(gU_{\alpha i})$: $(gU_{\alpha i}) \to (gU_{\alpha i}) \times F$, where F does not depend on the indices α or i. Figure 1 (center panel) depicts one of the many higher-order one-loop electroweak corrections, for illustrative purposes. The presence of new interactions changes the picture significantly as long as these have a nontrivial flavor structure. For example, a new interaction that involves only neutrinos and new degrees of freedom, depicted schematically in Fig. 1 (right panel), will modify the neutrino propagator and, in turn, modify $(gU_{\alpha i}) \to (gU_{\alpha i}) + \sum_j (gU_{\alpha j}) \times F_{ij}$. If the "loop factors" F_{ij} depend on i, $j = 1, 2, 3$, the $(gU_{\alpha i})$ change in a flavor-dependent way.

A simple, concrete model that would manifest itself in this way is adding a gauge-singlet scalar Φ to the SM field

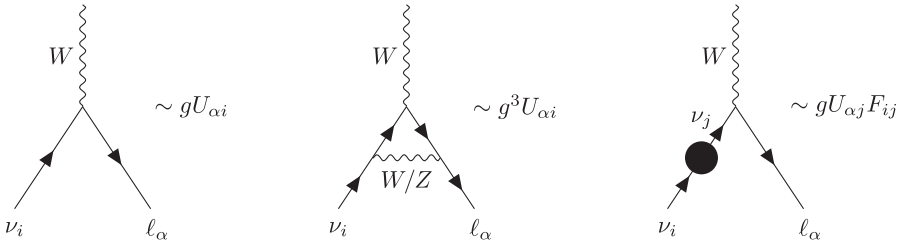

FIG. 1. Left: leading-order Feynman diagram for the W boson, charged lepton ℓ_α, neutrino ν_i coupling. Center: sample one-loop electroweak correction. This contribution is proportional to $(gU_{\alpha j})(gU^*_{\beta j})(gU_{\beta i}) = g^3U_{\alpha i}$ in the limit where the fermion masses are negligible and U is unitary. Right: sample one-loop correction from a new interaction that modifies the neutrino propagator. This contribution is proportional to $(gU_{\alpha j})F_{ij}$.

content and allowing for neutrino-scalar Yukawa interaction of the form $h_{ij}\Phi\bar{\nu}_i\nu_j$ (after electroweak symmetry breaking). Starting at the one-loop level, it is easy to see how the dark circle in Fig. 1 (right panel) is realized. This is not the model we explore here. Instead, we will concentrate on two ultraviolet-complete models,[2] introduced and discussed in more detail in Sec. IV.

Following the renormalization-group approach to capture the finite quantum corrections, when the dust settles, we assume that we can replace $(gU_{\alpha i}) \to (g(Q^2)U_{\alpha i}(Q^2))$ in a way that both g and U depend on the momentum transfer (squared) Q^2 that characterizes the interaction: both gauge coupling constant and the elements of the mixing-matrix run. Note that we are assuming that, for a fixed value of Q^2, $U_{\alpha i}(Q^2)$ can always be expressed as elements of a unitary matrix, so it is meaningful to discuss $U(Q^2)$ as a running mixing matrix. When discussing neutrino production or detection, it is often convenient to define the neutrino flavor eigenstates ν_α. The discussion above implies that, given the existence of the new, generation-dependent interactions, the neutrino flavor eigenstates are energy-scale dependent.

Neutrino flavor change as a function of the distance between source and detector depends on which linear combinations of ν_i couple to the different charged leptons for both the production and detection processes—the flavor eigenstates mentioned above—and on the differences of the squares of the neutrino masses. While quantum corrections also lead to running masses, in neutrino oscillations one is interested in the pole masses.[3] The reason is because we are interested in neutrinos that propagate a macroscopic distance. In the language of quantum field theory, the only contribution to the amplitude that characterizes neutrino production plus detection comes from on-shell neutrino exchange: the contributions from virtual neutrino exchange, to exquisite precision, cancel out. As a consequence of neutrinos being on shell, production and detection of neutrinos, which are associated with different energy scales, can be treated separately [41].

In summary, RG effects impact neutrino oscillations in the sense that they render the neutrino mixing matrix Q^2 dependent. We discuss flavor change in this context in great detail in the next section and return to concrete, phenomenologically safe models that lead to nontrivial $U(Q^2)$ in Sec. IV.

III. NEUTRINO OSCILLATION PHENOMENOLOGY

As discussed above, the new interactions of interest imply that the neutrino charged-current-weak-interaction eigenstates ν_e, ν_μ, and ν_τ depend on the scale of the neutrino-production and neutrino-detection processes. We can choose the scale of the couplings to be the so-called Lorentz-invariant "momentum transfer" Q^2: if we adopt all momenta in a vertex to be incoming, then $Q^2 \equiv |(p_\nu + p_\ell)^2|$, where p_ν and p_ℓ are, respectively, the momenta of the neutrino and charged lepton involved in the charged-current process of interest. For example, in $\pi \to \mu\nu_\mu$ we have $Q^2 = m_\pi^2$. In general, in a physics process characterized by Q^2 where a charged lepton ℓ_α ($\alpha = e$, μ, and τ) is absorbed and a neutrino is produced, the coherent linear combination of neutrino mass eigenstates ν_i ($i = 1, 2, 3$) produced is

$$\nu_\alpha(Q^2) = U_{\alpha i}(Q^2)\nu_i. \tag{3.1}$$

We are interested in neutrinos that propagate a finite distance so, as discussed in the previous section, when referring to neutrino mass eigenstates, we always refer to on-shell mass eigenstates with on-shell masses m_i, that is $\nu_i \equiv \nu_i(Q^2 = m_{\nu_i}^2)$. Note that we assume neutrinos are always produced and detected via the charged-current weak interactions.

In vacuum, a neutrino mass eigenstate with energy E is an eigenstate of the propagation Hamiltonian H. Its evolution, assuming that the neutrino is ultrarelativistic, has the familiar form

[2]The gauge-invariant realization of the $\Phi\bar{\nu}\nu$ operators is not renormalizable.

[3]The running mass should be used in evaluating the neutrino production and detection processes. Neutrino masses, however, are small enough that their impact is negligible in virtually all processes of interest.

$$|\nu_i(L)\rangle = \exp[-im_i^2 L/2E]|\nu_i(0)\rangle, \tag{3.2}$$

where L is the distance propagated or the baseline. The Dirac bracket notation refers to the flavor wave function of the neutrino state (e.g., a three-dimensional Hilbert space assuming there are three independent neutrino states). The probability $P_{\alpha\beta}$ that a neutrino is produced associated with a charged lepton ℓ_α in a process characterized by Q_p^2 and detected, a distance L away, in association with a charged lepton ℓ_β in a process characterized by Q_d^2 can be trivially, but carefully, computed as

$$\begin{aligned} P_{\alpha\beta}(L) &= |\langle \nu_\beta(Q_d^2)| \exp[-iHL]|\nu_\alpha(Q_p^2)\rangle|^2 \\ &= \left|\sum\nolimits_i U_{\beta i}(Q_d^2) U_{\alpha i}^*(Q_p^2) \exp[-im_i^2 L/2E]\right|^2. \end{aligned} \tag{3.3}$$

If the kinematics of the production and detection processes are the same, we obtain the familiar vacuum neutrino oscillation expressions. In general, however, this is not the case. Imagine an experimental setup where neutrinos are produced in charged-pion decay: $\pi^+ \to \mu^+\nu$. In this case, $Q_p^2 = m_\pi^2$, independent from the pion and neutrino laboratory energies. Further imagine that the neutrino is detected via $\nu + n \to e^- + p$. In the neutron's rest frame, for large enough neutrino energies, $Q_d^2 \sim Em_n$; Q_d^2 depends on the neutrino detector-frame energy and, clearly, has no relation to the pion mass. In the subsections that follow, we explore the consequences and subtleties of Eq. (3.3) and discuss how to handle the propagation of neutrinos through matter when the mixing matrix is Q^2 dependent.

Before proceeding, we wish to highlight that, for a fixed value of Q_p^2 and Q_d^2, the oscillation formalism we will explore here is similar to what one would obtain when considering the hypothesis that there is new physics in neutrino production and detection, and that the impact of new physics is process and flavor dependent [42] (for a more recent discussion, see also Ref. [43]). The two scenarios, however, are not identical since, in the setup under consideration here, there are different mixing matrices for different neutrino-scattering energies, even if the physics processes in question are the same; our U_α depend on the momentum transfer, not the nature of the neutrino-production and neutrino-detection processes. As an aside, our discussion here is a little more complete relative to the one in Ref. [42] as we look into three-flavor effects, matter effects, and new CP-violating phenomena more carefully.

A. Vacuum oscillations: Two and more flavors

We first consider the simplified case of two charged leptons and two neutrinos—e, μ, ν_1, and ν_2 for concreteness—propagating in vacuum. The most general two-by-two Q^2-dependent mixing matrix can be expressed as

$$\begin{aligned} U(Q^2) = &\begin{pmatrix} 1 & 0 \\ 0 & e^{i\gamma(Q^2)} \end{pmatrix} \begin{pmatrix} \cos\theta(Q^2) & \sin\theta(Q^2) \\ -\sin\theta(Q^2) & \cos\theta(Q^2) \end{pmatrix} \\ &\times \begin{pmatrix} e^{i\tilde{\alpha}(Q^2)} & 0 \\ 0 & e^{i\tilde{\beta}(Q^2)} \end{pmatrix}, \end{aligned} \tag{3.4}$$

where we indicate the Q^2 dependency of the mixing parameters γ, θ, $\tilde{\alpha}$, $\tilde{\beta}$ explicitly. Not all of these parameters are physical. We can redefine, with impunity, the kets $|\nu_e(Q^2)\rangle \to \exp[i\zeta(Q^2)]|\nu_e(Q^2)\rangle$ and $|\nu_\mu(Q^2)\rangle \to \exp[i\eta(Q^2)]|\nu_\mu(Q^2)\rangle$, for every value of Q^2, such that two among three complex phases can be removed. For example,

$$U(Q^2) = \begin{pmatrix} \cos\theta(Q^2) & \sin\theta(Q^2) \\ -\sin\theta(Q^2) & \cos\theta(Q^2) \end{pmatrix} \begin{pmatrix} 1 & 0 \\ 0 & e^{i\tilde{\beta}(Q^2)} \end{pmatrix} \tag{3.5}$$

allows one to access the answer to all possible oscillation-related questions. Finally, we are allowed to also phase redefine the mass-eigenstate kets $|\nu_i\rangle$ with impunity. Hence, we can choose $\tilde{\beta}(Q^2)$ in Eq. (3.5) to vanish at some *fixed* value of Q^2. In the most general case, therefore, the oscillation probabilities in Eq. (3.3) will depend on one mass-squared difference $\Delta m^2 \equiv m_2^2 - m_1^2$ and three mixing parameters,

$$\theta(Q_p^2) \equiv \theta_p, \qquad \theta(Q_d^2) \equiv \theta_d, \quad \text{and} \quad \tilde{\beta}(Q_d^2) - \tilde{\beta}(Q_p^2) \equiv \beta. \tag{3.6}$$

Throughout, in order to unambiguously define the mass eigenstates, we choose $m_2 > m_1$.

A different subtlety lies in the physical range for the mixing parameters. Q^2-dependent sign redefinitions of $|\nu_e\rangle$ and $|\nu_\mu\rangle$ allow one to choose, for example, $\theta(Q^2) \in [-\pi/2, \pi/2]$. Sign redefinitions of the mass eigenstates allow one to constrain θ to a specific quadrant [for example, $\theta(Q^2) \in [0, \pi/2]$] for some fixed value of Q^2. Hence, if we choose θ_p to lie in the first quadrant, there is no guarantee that the same will be true of θ_d.

Before proceeding, we wish to point out that the phase $\tilde{\beta}(Q^2)$ in Eq. (3.5) bears a strong resemblance to the so-called Majorana phase. However, they are not the same and should not be confused. Majorana phases are only physical when neutrinos are Majorana fermions and only manifest themselves in phenomena related, directly or indirectly, to lepton-number violation. The relative phase β manifests itself in ordinary flavor conversions and has nothing to do with lepton-number violation. It is physical for both Majorana and Dirac neutrinos. It is fair to ask about the origin and interpretation of this CP-odd new-physics parameter and why it impacts neutrino oscillations even

when there are only two families of leptons. One way to understand it is as follows. With two families and assuming the massive neutrinos are Dirac fermions, the weak-interaction couplings and the fermion masses can be chosen real. In the model under consideration here, however, there are more flavor-dependent interactions. If there are CP-violating couplings in the new-physics sector, those will manifest themselves at higher-order in charged-current processes and can mediate CP-violating effects. In oscillation language, these are parametrized by the (running) CP-odd phase β introduced above. Incidentally, it is trivial to show using Eqs. (3.3) and (3.5) that the effect of β in the oscillation probabilities in vacuum is to "shift" the oscillation phase: $\Delta m^2 L/2E \to \Delta m^2 L/2E + \beta$.

With all this in mind, for two flavors, Eq. (3.3) can be expressed as

$$P_{e\mu} = P_{\mu e} = \sin^2(\theta_p - \theta_d) + \sin 2\theta_p \sin 2\theta_d \sin^2\left(\frac{\Delta m^2 L}{4E} + \frac{\beta}{2}\right), \quad (3.7)$$

and

$$P_{ee} = P_{\mu\mu} = \cos^2(\theta_p - \theta_d) - \sin 2\theta_p \sin 2\theta_d \sin^2\left(\frac{\Delta m^2 L}{4E} + \frac{\beta}{2}\right). \quad (3.8)$$

The equality of $P_{\mu e}$ and $P_{e\mu}$ and P_{ee} and $P_{\mu\mu}$ is a consequence of the unitary evolution of the neutrino states and the fact that $|\nu_e(Q^2)\rangle$ and $|\nu_\mu(Q^2)\rangle$, for any Q^2, are a complete basis for the two-dimensional Hilbert space.[4] This is independent from the presence of the complex relative phase β. However, $P_{\mu e} = P_{e\mu}$ does not mean that T invariance is guaranteed. More carefully, Eq. (3.7) states that $P(\nu_e(Q_p^2) \to \nu_\mu(Q_d^2)) = P(\nu_\mu(Q_p^2) \to \nu_e(Q_d^2))$. T invariance is the statement $P(\nu_e(Q_p^2) \to \nu_\mu(Q_d^2)) = P(\nu_\mu(Q_d^2) \to \nu_e(Q_p^2))$. $P(\nu_\mu(Q_d^2) \to \nu_e(Q_p^2))$ is given by Eq. (3.7) with $\theta_d \leftrightarrow \theta_p$ and $\beta \to -\beta$ so T invariance is violated if $\beta \neq 0, \pi$.

For antineutrinos, $P_{\bar\alpha\bar\beta}(\theta_p, \theta_d, \beta) = P_{\alpha\beta}(\theta_p, \theta_d, -\beta)$ so CP invariance is also violated if $\beta \neq 0, \pi$. Note that, in general, $P_{\alpha\alpha} \neq P_{\bar\alpha\bar\alpha}$, which could be interpreted as an *apparent* violation of CPT. However, this does not signal violation of the CPT theorem since CPT invariance implies $P(\nu_\alpha(Q_p^2) \to \nu_\alpha(Q_d^2)) = P(\bar\nu_\alpha(Q_d^2) \to \bar\nu_\alpha(Q_p^2))$, which is satisfied.

For $Q_d^2 = Q_p^2$, we recover the well-known two-flavor oscillation expressions. In general, however, the situation is qualitatively different. For example, in the limit $L \to 0$, flavor is violated if either $\theta_p \neq \theta_d$ or $\beta \neq 0$. This is easy to understand. In either case, the mixing matrices are different at different values of Q^2 so the linear combinations of neutrinos that couple to e and μ are different: $\langle \nu_\alpha(Q_d^2)| \nu_\beta(Q_p^2)\rangle \neq \delta_{\alpha\beta}$. These zero-baseline effects, in practice, will constrain running effects to be relatively small, as we discuss more quantitatively in Sec. V. The complex relative phase β, in turn, leads to a phase shift in the oscillatory phenomenon. This leads, for example, to different behaviors of the oscillation probabilities at zero and small baselines. At zero baseline, a small β still induces an oscillation phase and thus $P_{\alpha\gamma} = \delta_{\alpha\gamma} + \mathcal{O}(\beta^2)$. At small-but-finite baseline L, while the standard oscillation probability goes as $P_{\alpha\gamma}^{\rm std} \sim \delta_{\alpha\gamma} + \mathcal{O}(\Delta_{ij}^2)$, a nonzero β would induce $P_{\alpha\gamma} \sim \mathcal{O}(\beta\Delta_{ij})$, where we have defined $\Delta_{ij} \equiv \Delta m_{ij}^2 L/2E$.

In the limit where the running effects are small, it is easier to appreciate analytically the impact of the new-physics effects. Assuming $\theta_d - \theta_p = \epsilon_\theta + \mathcal{O}(\epsilon_\theta^2)$ and $\beta = \epsilon_\beta + \mathcal{O}(\epsilon_\beta^2)$, both $\epsilon_\theta, \epsilon_\beta \ll 1$ and unrelated to one another,

$$P_{e\mu} = P_{\mu e} = \epsilon_\theta^2 + \mathcal{O}(\epsilon_\theta^4) + [\sin^2 2\theta_d - \sin 4\theta_d \epsilon_\theta + \mathcal{O}(\epsilon_\theta^2)] \times \left[\sin^2\left(\frac{\Delta m^2 L}{4E}\right) + \frac{\epsilon_\beta}{2}\sin\left(\frac{\Delta m^2 L}{2E}\right) + \mathcal{O}(\epsilon_\beta^2)\right] \quad (3.9)$$

and

$$P_{ee} = P_{\mu\mu} = 1 - \epsilon_\theta^2 + \mathcal{O}(\epsilon_\theta^4) - (\sin^2 2\theta_d - \sin 4\theta_d \epsilon_\theta + \mathcal{O}(\epsilon_\theta^2)) \times \left[\sin^2\left(\frac{\Delta m^2 L}{4E}\right) + \frac{\epsilon_\beta}{2}\sin\left(\frac{\Delta m^2 L}{2E}\right) + \mathcal{O}(\epsilon_\beta^2)\right]. \quad (3.10)$$

In the zero-baseline limit, the new-physics effects are $\mathcal{O}(\epsilon_\theta^2, \epsilon_\beta^2)$, quadratically small in the limit $\epsilon_\theta, \epsilon_\beta \ll 1$. For a finite baseline, instead, the new-physics effects are $\mathcal{O}(\epsilon_\theta, \epsilon_\beta)$. For example,

$$P_{e\mu} = P_{\mu e} = (\sin^2 2\theta_d - \epsilon_\theta \sin 4\theta_d)\sin^2\left(\frac{\Delta m^2 L}{4E}\right) + \frac{\epsilon_\beta}{2}\sin^2 2\theta_d \sin\left(\frac{\Delta m^2 L}{2E}\right) + \mathcal{O}(\epsilon_\theta^2, \epsilon_\beta^2, \epsilon_\theta\epsilon_\beta). \quad (3.11)$$

If the effects of mixing-angle running are not large, long-baseline experiments are, in some sense, more sensitive than short-baseline experiments.

The case of three charged leptons and neutrinos—e, μ, τ, ν_1, ν_2, ν_3—is straightforward but more cumbersome. Taking advantage of the invariance of observables on the overall phases of $|\nu_\alpha(Q^2)\rangle$, $\alpha = e, \mu, \tau$ and $|\nu_i\rangle$, $i = 1, 2, 3$, the most general 3×3 Q^2-dependent mixing matrix can be parametrized as

[4] In the two neutrino framework, one can show that $P_{ee} + P_{e\mu} = 1$ and $P_{ee} + P_{\mu e} = 1$. These translate into $P_{\mu e} = P_{e\mu}$.

$$U(Q^2) = \begin{pmatrix} 1 & 0 & 0 \\ 0 & c_{23}(Q^2) & s_{23}(Q^2) \\ 0 & -s_{23}(Q^2) & c_{23}(Q^2) \end{pmatrix} \begin{pmatrix} c_{13}(Q^2) & 0 & s_{13}(Q^2)e^{-i\delta(Q^2)} \\ 0 & 1 & 0 \\ -s_{13}(Q^2)e^{i\delta(Q^2)} & 0 & c_{13}(Q^2) \end{pmatrix} \tag{3.12}$$

$$\times \begin{pmatrix} c_{12}(Q^2) & s_{12}(Q^2) & 0 \\ -s_{12}(Q^2) & c_{12}(Q^2) & 0 \\ 0 & 0 & 1 \end{pmatrix} \begin{pmatrix} 1 & 0 & 0 \\ 0 & e^{i\tilde{\alpha}(Q^2)} & 0 \\ 0 & 0 & e^{i\tilde{\beta}(Q^2)} \end{pmatrix}, \tag{3.13}$$

where $c_{ij}(Q^2)$, $s_{ij}(Q^2)$ are shorthand for $\cos\theta_{ij}(Q^2)$, $\sin\theta_{ij}(Q^2)$, respectively, for $ij = 12, 13, 23$. The complex phases $\tilde{\alpha}(Q^2)$ and $\tilde{\beta}(Q^2)$ can be chosen such that they vanish at some value of Q^2.

The vacuum oscillation probabilities will be given by Eq. (3.3) with the elements of the mixing matrix as defined in Eq. (3.13). These will depend on the usual mass-squared differences $\Delta m^2_{31} \equiv m^2_3 - m^2_1$ and $\Delta m^2_{21} = m^2_2 - m^2_1$ (the third mass-squared difference is not independent, $\Delta m^2_{32} \equiv m^2_3 - m^2_2 = \Delta m^2_{31} - \Delta m^2_{21}$), six mixing angles $\theta_{ij}(Q^2_p)$, $\theta_{ij}(Q^2_d)$, $ij = 12$, 13, 23, two "Dirac" phases $\delta(Q^2_p)$, $\delta(Q^2_d)$, and two additional complex-phase differences, $\alpha \equiv \tilde{\alpha}(Q^2_d) - \tilde{\alpha}(Q^2_p)$ and $\beta \equiv \tilde{\beta}(Q^2_d) - \tilde{\beta}(Q^2_p)$. As in the two neutrino case, α and β will induce a shift in the solar and atmospheric oscillation phases: $\Delta_{21} \to \Delta_{21} + \alpha$, $\Delta_{31} \to \Delta_{31} + \beta$, and $\Delta_{32} \to \Delta_{32} + \beta - \alpha$. The mass eigenstates can be unambiguously defined in a variety of ways. Here, it pays off to adopt a definition that does not depend on the mixing matrix in order to avoid a Q^2-dependent definition. Concretely, we take the standard definition: $m^2_2 > m^2_1$ and $|\Delta m^2_{31}| > \Delta m^2_{21}$. $\Delta m^2_{31} > 0$ defines the "normal" mass ordering, and $\Delta m^2_{31} < 0$ defines the "inverted" one.[5]

The expressions for the oscillation probabilities for three flavors in the Q^2-dependent case are lengthy. We have nevertheless found several features in the zero-baseline limit and in the limit of small RG effects that turn out to be instructive. Let us first turn to the expressions in the zero-baseline ($L = 0$) limit. For simplicity, we take $\theta_{13} = 0$ and $\theta_{23} = \pi/4$ at production and assume that the difference between various parameters at different scales is small. We define $\epsilon_{ij} \equiv \theta_{ij}(Q^2_d) - \theta_{ij}(Q^2_p)$, $\epsilon_\delta = \delta(Q^2_d) - \delta(Q^2_p)$, $\epsilon_\alpha = \alpha$, and $\epsilon_\beta = \beta$. Note that $|\alpha|, |\beta| \ll 2\pi$. Hence, ϵ_{ij} is the amount the angle runs between momentum transfers corresponding to production and detection. We omit the "production" subscript and thus it should be understood that all angles in the expressions below correspond to the momentum scale of neutrino production. Finally, below, we keep up to quadratic terms in all ϵ's. This leads to the zero-baseline survival probabilities

$$\begin{aligned} P_{ee} &\simeq \left| 1 - \frac{\epsilon^2_{12} + \epsilon^2_{13}}{2} - \frac{\epsilon^2_\alpha}{2} s^2_{12} + i\epsilon_\alpha s^2_{12} \right|^2 \\ &\simeq 1 - \epsilon^2_{12} - \epsilon^2_{13} - \frac{1}{4}\epsilon^2_\alpha \sin^2 2\theta_{12}, \end{aligned} \tag{3.14}$$

and

$$\begin{aligned} P_{\mu\mu} &= \Big| 1 - \frac{1}{4}(\epsilon^2_{12} + \epsilon^2_{13} + 2\epsilon^2_{23} + \epsilon^2_\alpha c^2_{12} + \epsilon^2_\beta - \epsilon_{13}\epsilon_\alpha s_\delta \sin 2\theta_{12} \\ &\quad + 2\epsilon_{12}\epsilon_{13} c_\delta) + \frac{i}{2}(\epsilon_\alpha c^2_{12} + \epsilon_\beta) \Big|^2 \\ &\simeq 1 - \frac{1}{4}(\epsilon_\beta - \epsilon_\alpha c^2_{12})^2 - \epsilon^2_{23} - \frac{1}{2}(\epsilon_\alpha c_{12} s_{12} - \epsilon_{13} s_\delta)^2 \\ &\quad - \frac{1}{2}(\epsilon_{12} + \epsilon_{13} c_\delta)^2, \end{aligned} \tag{3.15}$$

where $c_\delta = \cos\delta$ and $s_\delta = \sin\delta$.

On the other hand, zero-baseline appearance probabilities include

$$\begin{aligned} P_{\mu e} &\simeq \frac{1}{2}|\epsilon_{13} + e^{i\delta}(\epsilon_{12} + i\epsilon_\alpha c_{12} s_{12})|^2 \\ &\simeq \frac{1}{8}\epsilon^2_\alpha \sin^2 2\theta_{12} - \frac{\epsilon_\alpha \epsilon_{13}}{2} \sin 2\theta_{12} s_\delta + \frac{\epsilon^2_{12} + \epsilon^2_{13}}{2} + \epsilon_{12}\epsilon_{13} c_\delta, \\ P_{\mu\tau} &\simeq \left| \epsilon_{23} + \frac{i}{2}(\epsilon_\alpha c^2_{12} - \epsilon_\beta) \right|^2 = \epsilon^2_{23} + \frac{1}{4}(\epsilon_\alpha c^2_{12} - \epsilon_\beta)^2. \end{aligned} \tag{3.16}$$

As already inferred in the case of two flavors, the RG effects at zero baseline appear at $\mathcal{O}(\epsilon^2)$, which is clear from Eqs. (3.14)–(3.16). Moreover, it is trivial to show that all asymmetries $P_{\alpha\beta} - P_{\bar{\alpha}\bar{\beta}}$ are exactly zero at zero baseline (without any approximations).

For a finite baseline, even approximate expressions for the oscillation probabilities are rather lengthy (full expressions may be found in [44]), so here we focus on asymmetries. We keep terms linear in ϵ and up to order

[5] A different choice would have been $|U_{e1}(Q^2)|^2 > |U_{e2}(Q^2)|^2 > |U_{e3}(Q^2)|^2$. This clearly depends on Q^2 and may lead to confusion. There is nothing wrong, however, with using something like $|U_{e1}(Q^2 = 0)|^2 > |U_{e2}(Q^2 = 0)|^2 > |U_{e3}(Q^2 = 0)|^2$.

s_{13}^2 or $\Delta m_{21}^2/\Delta m_{31}^2$, assuming that the oscillation phase is near the atmospheric maximum. Moreover, for terms that are order ϵ we only keep terms that are at most linear in s_{13} or $\Delta m_{21}^2/\Delta m_{31}^2$. The muon neutrino disappearance asymmetry in vacuum is, for example,

$$P_{\mu\mu} - P_{\bar{\mu}\bar{\mu}} \simeq \{-(\epsilon_\alpha c_{12}^2 - \epsilon_\beta)\sin^2 2\theta_{23} + 8\epsilon_{12} c_{13}^2 s_{13} c_{23} s_{23}^3 s_\delta - \epsilon_\delta s_{23}^4 \sin^2 2\theta_{13}\} \sin\Delta_{31} - \epsilon_{13} \sin 2\theta_{12} \sin 2\theta_{23} s_\delta \times (1 + s_{23}^2 \cos\Delta_{31}) \sin\Delta_{21}. \quad (3.17)$$

We will see later that θ_{12} typically runs more than other angles and phases in the scenarios we will study, so we call attention to the fact that the ϵ_{12} term in the asymmetry above is suppressed by s_{13}. The dependence on ϵ_α and ϵ_β is relatively large. As already stressed in the two-flavor scenario, at finite baseline there are effects already at $\mathcal{O}(\epsilon)$; compare, for instance, Eq. (III.17) with Eqs. (3.14)–(3.16).

The electron neutrino disappearance asymmetry is given by

$$P_{ee} - P_{\bar{e}\bar{e}} \simeq (\epsilon_\beta - \epsilon_\delta)\sin^2 2\theta_{13} \sin\Delta_{31} - \epsilon_\alpha (s_{12}^2 \sin^2 2\theta_{13} \sin\Delta_{31} - \sin^2 2\theta_{12} \sin\Delta_{21}). \quad (3.18)$$

This expression does not depend on ϵ_{12}, ϵ_{13}, and ϵ_{23} to order s_{13}^2 or Δ_{21}. The formulas for P_{ee} and $P_{\bar{e}\bar{e}}$, however, do contain those: the effects cancel in the difference $P_{ee} - P_{\bar{e}\bar{e}}$. Hence, by studying differences between electron neutrino and electron antineutrino disappearances, one can access RG induced effects on phases. As discussed, the apparent violation of CPT symmetry can be seen from Eqs. (III.17) and (III.18), since the differences between neutrino and antineutrino disappearance are, in principle, not zero. These differences are CP odd, as they change sign under the reversal of the signs of all the phases.

The difference between electron neutrino and antineutrino appearance probabilities in a muon (anti)neutrino "beam" is somewhat lengthy. Concentrating on the dominant terms up to order s_{13} and dropping Δ_{21} terms multiplied by new-physics contributions, we obtain

$$P_{\mu e} - P_{\bar{\mu}\bar{e}} \simeq -8J\Delta_{21}\sin^2\left(\frac{\Delta_{31}}{2}\right) \times \left[1 + \left(2\frac{\epsilon_{12}}{\sin 2\theta_{12}} + \epsilon_\alpha \frac{c_\delta}{s_\delta}\right)\frac{\cot(\Delta_{31}/2)}{\Delta_{21}}\right], \quad (3.19)$$

where $J = c_{13}^2 s_{13} c_{12} s_{12} c_{23} s_{23} \sin\delta$ is the Jarlskog invariant [45,46]. At long-baseline experiments, where this channel matters the most, such expansion is reasonable and accurate (ignoring the matter effects). We see that in Eq. (III.19) there is also a term that is ϵ independent; that is the standard CP-violating term. Interestingly, although the terms containing ϵ_{12} and ϵ_α are enhanced by $\sim\Delta_{31}/\Delta_{21}$, at the peak of the "atmospheric" oscillation $\cot\Delta_{31}/2 \simeq \cot\pi/2 = 0$, which suppresses the CP-violating effect. This is particularly pronounced for the T2K setup as will be seen in Sec. V. We also stress that, in the $\delta \to 0$ limit, in which there is no standard CP violation in the lepton sector, new RG induced CP violation is still present and nonzero (ϵ_α term). In the future, comparing the amount of leptonic CP violation in DUNE and T2HK will allow one to probe this scenario thanks to the different neutrino energy spectra at the two experiments.

In order to highlight the CP-conserving contribution, the sum of the electron neutrino and electron antineutrino appearance probabilities, for $\Delta_{21} \to 0$, is

$$P_{\mu e} + P_{\bar{\mu}\bar{e}} = 2\sin^2 2\theta_{13} s_{23}^2 \left[1 + 2\epsilon_{13}\frac{\cos 2\theta_{13}}{\sin 2\theta_{13}} - \frac{c_{23}}{s_{13} s_{23}} \times (\epsilon_{12} c_\delta - \epsilon_\alpha c_{12} s_{12} s_\delta)\right] \sin^2\left(\frac{\Delta_{31}}{2}\right). \quad (3.20)$$

The first term is the dominant component of the standard contribution. It is interesting to observe that the effect of new physics is enhanced by $1/s_{13} \sim 7$. A change in $P_{\mu e} + P_{\bar{\mu}\bar{e}}$ can be compensated, in this channel, by shifting the value of $\sin^2\theta_{23}$ or $\sin^2 2\theta_{13}$. Therefore a mismatch between the θ_{23} value measured in the ν_μ disappearance mode versus the ν_e appearance mode or a mismatch between θ_{13} values measured at reactor neutrino experiments and beam ν_e appearance are signatures of our scenario. From Eqs. (III.19) and (III.20), we can infer that the current measurements of electron neutrino appearance by T2K [47] and NOνA [48] should already constrain ϵ_{12}, ϵ_{13}, and ϵ_α to be below, roughly, 10%.

We summarize the qualitative effects of the running of the mixing matrix on neutrino oscillation phenomenology and provide some of the most promising and direct experimental probes of this scenario below:

(i) In general, the mismatch between the production and detection mixing matrices affects all neutrino oscillation channels.
(ii) The effect of the phase differences, α and β [see Eq. (III.13)], is a shift of the solar (Δ_{21}) and atmospheric (Δ_{31}) oscillation phases, respectively.
(iii) Zero-baseline transitions happen at second order in the new-physics parameters. Nonetheless, searches for short-baseline oscillations provide good experimental probes of this scenario, particularly if performed at high neutrino energies, which makes the neutrino production and detection scales more distinct.
(iv) The impact of the running of the mixing matrix on long-baseline oscillation probabilities is first order in

the new-physics parameters and thus the determination of the same oscillation parameters at different scales and the precise energy dependence of the oscillation probability curves are promising venues for probing this scenario.

(v) Mixing-matrix running may lead to apparent *CPT* violation: $P_{\alpha\alpha} - P_{\bar{\alpha}\bar{\alpha}}$ is, in general, nonzero for a finite baseline. *CPT* symmetry is, of course, still conserved. These asymmetries, or perhaps the ratios $(P_{\alpha\alpha} - P_{\bar{\alpha}\bar{\alpha}})/(P_{\alpha\alpha} + P_{\bar{\alpha}\bar{\alpha}})$, could be powerful probes of mixing-matrix running, especially due to possible cancellations of systematic uncertainties.

(vi) Mixing-matrix running may also affect appearance channels in *CP*-violating and *CP*-conserving ways. Long-baseline experiments yielding different neutrino energy ranges, including Noνa, T2K, DUNE, and T2HK, could be sensitive to this scenario. Two experimental signatures stand out in the case of electron appearance: a mismatch between θ_{13} values measured at reactor and accelerator neutrino experiments, or a disagreement on the θ_{23} values measured in appearance and disappearance modes in beam neutrino experiments. In fact, current Noνa and T2K data are expected to be already sensitive to new sources of *CP* violation, potentially constraining ϵ_{12} and ϵ_α to be below 10% or so.

B. Matter effects: Two and more flavors

Neutrino flavor evolution is modified in the presence of matter. The Hamiltonian that describes flavor evolution as a function of the baseline is

$$H = \sum_i \frac{m_i^2}{2E} |\nu_i\rangle\langle\nu_i| + A(L)|\nu_e(Q^2 = 0)\rangle\langle\nu_e(Q^2 = 0)|, \tag{3.21}$$

where $A(L) = \sqrt{2} G_F N_e(L)$ is the matter potential, G_F is the Fermi constant, and N_e is the electron number density of the medium as a function of the baseline. The matter potential is a coherent forward scattering phenomenon where the neutrinos interact with the electrons in the medium at zero momentum transfer. Hence, the ν_e interaction state of interest here is the one at $Q^2 = 0$. H can be expressed in any basis of the Hilbert space, as usual. Here, there are several tempting ones: the mass-eigenstate basis, the interaction basis "at production" and the interaction basis "at detection." The mass-eigenstate basis is especially useful since it allows one to readily compute the flavor evolution for arbitrary values of Q_p^2 and Q_d^2. The fact that H depends on $\nu_e(Q^2 = 0)$ also induces a natural choice for the complex phases $\tilde{\alpha}, \tilde{\beta}$, defined in Eq. (3.13): $\tilde{\alpha}(Q^2 = 0) = \tilde{\beta}(Q^2 = 0) = 0$.

It is instructive to discuss the case of two flavors and a constant $A(L) = A$, which can be solved analytically. Using Eq. (3.5) and defining $\theta_0 = \theta(Q^2 = 0)$ and setting $\tilde{\beta}(Q^2 = 0) = 0$, the eigenstates of the propagation Hamiltonian are

$$|\nu_{1M}\rangle = \cos\omega|\nu_1\rangle - \sin\omega|\nu_2\rangle, \tag{3.22}$$

$$|\nu_{2M}\rangle = \sin\omega|\nu_1\rangle + \cos\omega|\nu_2\rangle, \tag{3.23}$$

where

$$\sin 2\omega = \frac{A}{\Delta_M}\sin 2\theta_0, \tag{3.24}$$

$$\cos 2\omega = \frac{(\Delta - A\cos 2\theta_0)}{\Delta_M}, \tag{3.25}$$

$$\Delta_M = [(\Delta - A\cos 2\theta_0)^2 + A^2\sin^2 2\theta_0]^{1/2}, \tag{3.26}$$

and $\Delta = \Delta m^2/(2E)$. Δ_M is the difference between the eigenvalues associated with $|\nu_{2M}\rangle$ and $|\nu_{1M}\rangle$; $|\nu_{2M}\rangle$ is associated with the larger eigenvalue when $A > 0$. We labeled the "matter mixing angle" ω in order to remind the reader that these states are expressed in the mass basis, not, as one is most familiar, in the interaction basis.

It is straightforward but rather lengthy to compute $P_{e\mu} \equiv P(\nu_e(Q_p^2) \to \nu_\mu(Q_d^2))$. Given a $|\nu_e(Q_p^2)\rangle$ at $L = 0$, the flavor-state vector at L is

$$|\nu(L)\rangle = |\nu_{1M}\rangle\langle\nu_{1M}|\nu_e(Q_p^2)\rangle + |\nu_{2M}\rangle\langle\nu_{2M}|\nu_e(Q_p^2)\rangle e^{-i\Delta_M L}, \tag{3.27}$$

and hence

$$P_{e\mu} = |\langle\nu_\mu(Q_d^2)|\nu_{1M}\rangle\langle\nu_{1M}|\nu_e(Q_p^2)\rangle + \langle\nu_\mu(Q_d^2)|\nu_{2M}\rangle\langle\nu_{2M}|\nu_e(Q_p^2)\rangle e^{-i\Delta_M L}|^2. \tag{3.28}$$

The Dirac brackets in Eq. (3.28) are

$$\begin{aligned}
\langle\nu_{1M}|\nu_e(Q_p^2)\rangle &= \cos\theta_p\cos\omega - \sin\theta_p\sin\omega e^{i\tilde{\beta}_p},\\
\langle\nu_{2M}|\nu_e(Q_p^2)\rangle &= \cos\theta_p\sin\omega + \sin\theta_p\cos\omega e^{i\tilde{\beta}_p},\\
\langle\nu_{1M}|\nu_\mu(Q_d^2)\rangle &= -\sin\theta_d\cos\omega - \cos\theta_d\sin\omega e^{i\tilde{\beta}_d},\\
\langle\nu_{2M}|\nu_\mu(Q_d^2)\rangle &= -\sin\theta_d\sin\omega + \cos\theta_d\cos\omega e^{i\tilde{\beta}_d}.
\end{aligned} \tag{3.29}$$

Note that, since $P_{ee} + P_{e\mu} = 1$, the survival probability can be obtained trivially from the appearance one [Eq. (3.28) with help from Eqs. (3.29)].

For three flavors, one can approach the issue of matter effects following the same steps we outline above for two flavors. We especially highlight the usefulness of performing computations in the mass-eigenstate basis. Analytic results, even if one is willing to make several different simplifying assumptions, are very hard to come by and are

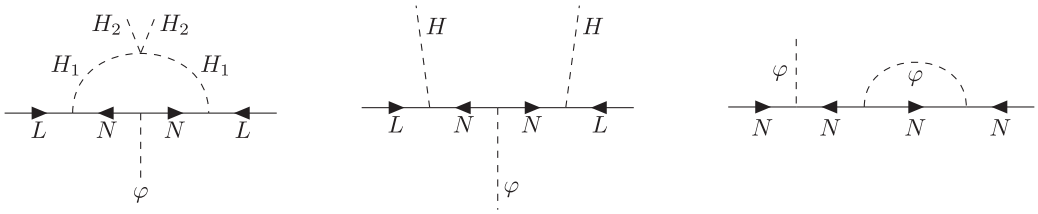

FIG. 2. Left: Feynman diagram associated with the generation of neutrino masses in a scotogeniclike neutrino mass model in which $\mathcal{M} \propto Y_N$ (model 1). Middle: Feynman diagram associated with the generation of neutrino masses in an inverse seesaw model in which $\mathcal{M} \propto Y_N^{-1}$ (model 2). Right: representative Feynman diagram responsible for the running of Y_N in both models 1 and 2. See text for details.

not illuminating. In Sec. V, we compute oscillation probabilities including running effects for different experimental setups. There, matter effects are always included and we do not make use of any approximate expressions; Eq. (III.21) is treated numerically.

IV. BENCHMARK MODELS

In Sec. II we discussed the concept of RG evolution in the low-energy neutrino sector without specifying a complete model. In order to discuss quantitative effects at neutrino experiments, however, it is useful to discuss ultraviolet-complete frameworks. We will focus on models that address the neutrino mass puzzle and in which the RG effects come from a "secluded sector." We concentrate on two simple models.

A. Model 1

First, we consider a variation of the scotogenic model [49] with a $U(1)$ lepton-number symmetry. The two Higgs doublets of the scotogenic model, H_1 and H_2, have zero lepton number but are distinguished by a $\mathbb{Z}_2$ symmetry under which H_1 is odd while H_2 is even. As in the original scotogenic model, lepton number and the $\mathbb{Z}_2$ symmetries allow the term $\lambda(H_1^\dagger H_2)^2 + \text{H.c.}$ in the scalar potential. The model also comprises three right-handed neutrinos N_R, with lepton number $+1$, which are odd under $\mathbb{Z}_2$. Finally, we add a complex scalar singlet φ, which is even under $\mathbb{Z}_2$ and has lepton number -2. The new-physics Lagrangian includes

$$-\mathcal{L}_\nu^{(1)} = \bar{L} Y_\nu \tilde{H}_1 N_R + \varphi \overline{N_R^c} Y_N N_R + \text{H.c.}, \tag{4.1}$$

where Y_ν and Y_N are matrices in generation space. The scalar potential is such that φ and H_2 develop vacuum expectation values (VEVs), while H_1 does not. The active neutrinos acquire Majorana masses, as depicted in the left panel of Fig. 2. The VEV of φ, $v_\varphi \equiv \langle \varphi \rangle$, in particular, breaks lepton number, but the $\mathbb{Z}_2$ symmetry remains unbroken. Therefore, the active neutrinos do not mix with the gauge singlets N_R. Breaking lepton number spontaneously would lead to a massless Goldstone boson, the Majoron [50]. In principle, the mass of the Majoron could be made nonzero by soft lepton-number breaking terms in the scalar potential, such as $\mu^2\varphi^2$.

Without loss of generality, Y_N can be taken as real, positive, and diagonal. Y_ν is a generic complex matrix. The neutrino mass matrix is given by

$$M_\nu^{ij} = \frac{\lambda v_\varphi}{8\sqrt{2}\pi^2} \sum_k \left\{ (Y_\nu^{ik} Y_\nu^{jk} Y_N^k) \left[\frac{M_H^2}{2M_H^2 - (Y_N^k v_\varphi)^2} \ln \frac{2M_H^2}{(Y_N^k v_\varphi)^2} - \frac{M_A^2}{2M_A^2 - (Y_N^k v_\varphi)^2} \ln \frac{2M_A^2}{(Y_N^k v_\varphi)^2} \right] \right\}, \tag{4.2}$$

where $M_{H,A}$ are the masses of the inert neutral scalar and pseudoscalar, respectively. Here, we are interested in light φ and N_R, and thus $v_\varphi \ll v \equiv 246$ GeV. In the limit of small N masses, i.e., $M_N^i = Y_N^i v_\varphi/\sqrt{2} \ll M_{H,A}$, Eq. (4.2) reduces to

$$M_\nu \simeq \frac{\lambda v_\varphi}{16\sqrt{2}\pi^2} Y_\nu Y_N Y_\nu^T \ln \frac{M_H^2}{M_A^2}. \tag{4.3}$$

The mixing matrix is defined via diagonalization $M_\nu^{\text{diag}} = U^\dagger M_\nu U^*$, where M_ν^{diag} is diagonal and contains the neutrino masses. We assume the inert doublet masses to be of order of the weak scale, so Y_ν does not run at low energies and can be treated as a constant parameter. Y_N, however, is scale dependent for values of the energy scale that are above the mass of the φ, N.

B. Model 2

The second benchmark model we will focus on is a version of the type-I seesaw mechanism [51–56], where the right-handed neutrino Majorana masses arise from the (possibly explicit) breaking of lepton number in the scalar potential. The model includes three SM singlet fermions N_R with lepton number 1, and a singlet scalar φ with lepton number -2. The Yukawa Lagrangian reads

$$-\mathcal{L}_\nu^{(2)} = \overline{L} Y_\nu \tilde{H} N_R + \varphi \overline{N_R^c} Y_N N_R + \text{H.c.}, \tag{4.4}$$

where H is the SM Higgs boson. The VEV of φ breaks lepton number.[6] The diagram generating neutrino masses for this model is presented in the middle panel of Fig. 2. When φ develops a VEV, active neutrinos acquire a mass matrix given by

$$M_\nu = \frac{\sqrt{2}v^2}{4v_\varphi} Y_\nu (Y_N)^{-1} Y_\nu^T. \tag{4.5}$$

The mixing matrix is defined as before but now the functional dependence of U on Y_N is distinct from the previous model, changing the impact of Y_N running qualitatively with respect to model 1.

For both models, it is straightforward to compute the scale dependence of Y_N. The right panel of Fig. 2 depicts a representative Feynman diagram that contributes to this running. The beta function of Y_N can easily be calculated and yields, for both models 1 and 2,

$$16\pi^2\beta(Y_N) \equiv 16\pi^2 \frac{dY_N}{d\ln|Q|} = 4Y_N\left[Y_N^2 + \frac{1}{2}\mathrm{Tr}(Y_N^2)\right]. \tag{4.6}$$

Any relatively large entry in Y_N can lead to a significant running of all Y_N entries and as a consequence to observable running of the mixing matrix.

Y_N is not directly related to the mixing matrix. In order to connect the running of Y_N and the running of the mixing matrix, we need to specify other Lagrangian parameters, including the Yukawa coupling matrices Y_ν (for both models). To achieve that, we make use of the Casas-Ibarra parametrization [57], which relates the Lagrangian parameters to the running leptonic mixing-matrix and neutrino masses,

$$Y_\nu = \frac{1}{\sqrt{C}} U^\dagger(Q_p^2) \sqrt{\mathrm{diag}(m_{\nu_1}, m_{\nu_2}, m_{\nu_3})} R Y_N^{-x/2}, \tag{4.7}$$

where C are the VEV-dependent prefactors in Eqs. (IV.3) and (IV.5) for model 1, when $x = 1$, and model 2, when $x = -1$, respectively. R is, in general, a complex orthogonal matrix and m_{ν_i} in the formula are masses at $Q^2 = m_\nu^2$ scale instead of running masses. Let us stress that the Y_ν matrix is not running across considered scales, since the scalar field that participates in such interaction is integrated out. In particular, we wish to stress that Eq. (IV.7) is evaluated only once, at the scale corresponding to the production and, in particular, before any running has been conducted.

[6]As in model 1, this would predict a Majoron. An active-neutrino–Majoron coupling would be induced. It, however, is doubly suppressed by $\nu - N$ mixing and m_ν/v_φ and could be very small (easily of order 10^{-9}) for the right-handed neutrino masses of interest. Hence the model is expected to be experimentally safe. Again, the Majoron could be given a nonzero mass via soft breaking terms in the scalar potential.

In the next section, when computing new-physics effects in oscillation experiments, we have the freedom to choose values for the elements of R and the constants that make up C. We will assume R to be real and parametrized by three Euler-like rotation angles ξ_1 in 1–2 plane, ξ_2 in 2–3 plane, and ξ_3 in 1–3 plane. The results we present below are not qualitatively different if we are to assume ξ_1, ξ_2, ξ_3 to be complex angles with magnitudes of order 1.

V. IMPACT ON NEUTRINO OSCILLATION EXPERIMENTS

Given the two concrete models outlined above, we proceed with the analysis of the impact of the running of the mixing-matrix elements at various neutrino experiments. Results for the two different models turn out to be qualitatively similar and the results presented below all correspond to model 1. We take this opportunity to stress one "advantage" of model 1, namely, the absence of mixing between active and sterile neutrinos. This makes it easier to satisfy experimental constraints on the mixing of the active neutrinos with the relatively light sterile neutrinos.

In Sec. V A, we discuss the signatures of the scenario at long-baseline experiments such as T2K [47,58,59] and Noνa [48,60,61], and then we confront these findings with the bounds from the short-baseline experiments NOMAD [62–64], ICARUS [65], CHARM-II [66], and NuTeV [67,68]. In Sec. V B, we focus on how this phenomenon impacts the flavor composition of astrophysical neutrinos measured by IceCube [69–71].

A. Long-baseline oscillation experiments

We assume that the masses of the new-physics particles are of order of the pion mass, so RG running of the mixing parameters is only relevant for Q^2 values larger than $(100\ \mathrm{MeV})^2$. For lower values of Q^2, one can treat the mixing parameters as constant. The reason is that we are mostly interested in neutrinos produced at values of $Q_p^2 \leq m_\pi^2$, since all beam neutrinos are predominantly produced in pion decay, and hence, at Q_p^2, the mixing matrix is the same for all experimental setups. Furthermore, for reactor and solar (anti)neutrino experiments, both Q_p^2 and Q_d^2 are less than the pion mass squared. Hence, we do not need to worry about running effects when it comes to extracting the current best-fit values of most mixing parameters, as we discuss in more detail below.

Different values for Y_ν at Q_p^2 are generated using Eq. (4.7) and the following:

(i) We fix $\sin^2\theta_{12}(Q_p^2) = 0.310$, $\sin^2\theta_{13}(Q_p^2) = 0.022$, and $\Delta m_{21}^2 = 7.53 \times 10^{-5}\ \mathrm{eV}^2$.

(ii) We choose the atmospheric parameters $\theta_{23}(Q_p^2)$ and $\Delta m_{31}^2(Q_p^2)$ at random, with a flat prior on their respective 3σ currently allowed regions according to NuFIT [72]. The reason for this choice is that

TABLE I. Reference values of neutrino energy and $\sqrt{Q_d^2}$ for all experiments considered here. For T2K and Noνa we take the peak of the neutrino spectra, while for all others (the short-baseline experiments) we use the average neutrino energy. The last two columns summarize the short-baseline constraints imposed (not applicable for T2K and Noνa). See text for details.

Experiment	E (GeV)	$\sqrt{Q_d^2}$ (GeV)	Channel	Constraint
T2K [47,58,59]	0.6	0.56	⋯	⋯
Noνa [48,60,61]	2.1	1.27	⋯	⋯
ICARUS [65]	17	3.94	$\nu_\mu \to \nu_e$	3.4×10^{-3}
CHARM-II [66]	24	4.70	$\nu_\mu \to \nu_e$	2.8×10^{-3}
NOMAD [62–64]	47.5	6.64	$\nu_\mu \to \nu_e$	7.4×10^{-3}
			$\nu_\mu \to \nu_\tau$	1.63×10^{-4}
			$\nu_\mu \to \nu_e$	5.5×10^{-4}
NuTeV [67,68]	250	15.30	$\nu_e \to \nu_\tau$	0.1
			$\nu_\mu \to \nu_\tau$	9×10^{-3}

atmospheric parameters are measured using experimental setups where Q_d^2 is larger than m_π^2, hence we allow for a relatively large range of values at Q_p^2.

(iii) We choose the CP-odd phases $\tilde{\alpha}(Q_p^2)$, $\tilde{\beta}(Q_p^2)$, and $\delta(Q_p^2)$ at random, with a flat prior, from their full allowed physical ranges.

(iv) We fix the value of the lightest neutrino mass and the neutrino mass ordering. We will show results for two values: 0.05 eV, marginally consistent with cosmological bounds on the sum of the active neutrino masses [73], and 0.01 eV. We will also show results for both normal ordering (NO) and inverted ordering (IO). Note that, quantitatively, effects depend considerably on the mass ordering and the lightest neutrino mass. It is well known, for example, that the RG effects are strongest for quasidegenerate masses [32].

(v) We choose the angles that parametrize the orthogonal R matrix at random, with a flat prior, from their full allowed physical ranges.

(vi) We pick the Yukawa matrix Y_N, at Q_p^2, to be $\mathrm{diag}(0.2, 0.5, 0.7)$. We have checked that the results of the scans are qualitatively independent from the choice of $Y_N(Q_P^2)$ as long as the couplings are nondegenerate and large enough to induce significant RG running.

As an aside, we have checked that the aforementioned choices for the couplings do not lead to the appearance of Landau poles below 10 TeV.

For each mass matrix defined at Q_p^2 as described above, we solve Eq. (IV.6) numerically and compute the mixing matrix at the different relevant values of Q_d^2. With that information, we compute the oscillation probabilities numerically, as discussed in detail in Sec. III, including matter effects. Throughout, we will use these randomly generated scenarios to discuss the reach of RG-running effects. A complete scan of the parameter space is not practically feasible given its dimensionality.

At detection, neutrinos interact mostly with the nucleons in the detectors through t-channel vector-boson exchange; the associated Q^2 can take any value in a continuous interval.[7] In order to estimate the RG effects accurately, Q_d^2 values should be extracted in an event-by-event basis. Our goals in this manuscript, however, are to illustrate the effects of the running of the mixing matrix in simple models that explain nonzero neutrino masses and to demonstrate that these can be observed in neutrino oscillation experiments. With this in mind, we take a simplified approach that should prove to be a good approximation statistically. In $2 \to 2$ scattering kinematics (see, e.g., Ref. [74]) the minimal and maximal values of $t = -Q^2$ are fixed, and thus we associate the mean value of the two to $-Q_d^2$. This yields $Q_d^2 = (2m_N E^2)/(2E + m_N)$, where m_N is the nucleon mass and E is the neutrino energy. We take E to be the average neutrino energy in short-baseline experiments, while for T2K and Noνa we study the impact of the running for the peak of their respective energy spectra. Table I lists the relevant energies and corresponding $\sqrt{Q_d^2}$ values for all experiments considered here.

The left panel of Fig. 3 depicts the biprobability plot at T2K (red points) and Noνa (blue points) for the NO, assuming the lightest neutrino mass to be $m_1 = 0.05$ eV, for 30,000 values of the model parameters, generated following the procedure described above. Note that here we do not take into consideration constraints from other experiments, to which we return momentarily. The panel also depicts the biprobabilities accessible in the absence of RG running (green for T2K, yellow for Noνa), for values of the atmospheric parameters Δm_{31}^2 and $\sin^2\theta_{23}$ picked at random (flat prior) from their respective 1σ currently allowed regions, according to NuFIT [72] and for values of δ also chosen at random from $\delta \in [0, 2\pi]$. The red and

[7]This is to be contrasted with what happens in s-channel scattering, where the Q^2 is defined by the incoming neutrino energy and the mass or energy fraction of the target particle.

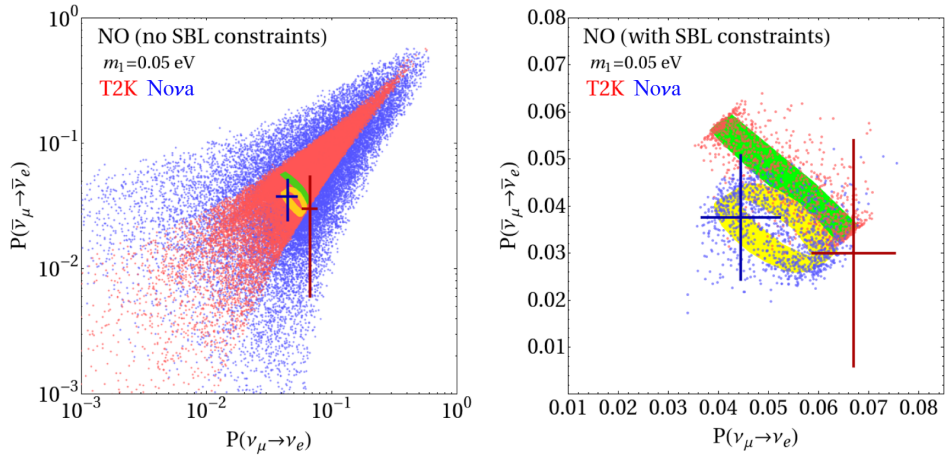

FIG. 3. Biprobability plots for NO and $m_1 = 0.05$ eV. Left: red and blue points are for T2K and Nova, respectively, for the case where RG effects are taken into account. These points are to be compared to the respective standard 1σ-allowed regions (green for T2K, yellow for Nova). Right: same as left, except that only points that satisfy the short-baseline (SBL) constraints are included. See text for details.

blue points with error bars represent the results of analyzing T2K and Nova data, respectively, adapted from Ref. [75]. Figure 3 reveals that running effects can be very significant; they lead to appearance probabilities that differ from "no-running" expectations by more than an order of magnitude. Effects at Nova are more pronounced because (a) the typical neutrino energies are larger at Nova and the mixing parameters have more "room" to run, and (b) at T2K, as discussed around Eq. (III.9), L/E values are such that CP-odd effects due to the new physics are suppressed.

As discussed in Sec. III, RG running leads to zero-baseline effects since, in general, $U(Q_p^2)U^\dagger(Q_d^2) \neq \mathbb{1}$. Therefore, experiments with very short baselines, designed, with the benefit of hindsight, for probing neutrino scattering physics or light sterile-neutrino phenomenology, are sensitive to this type of new physics. In particular, setups with high average neutrino energy are especially sensitive due to the larger difference between Q_p^2 and Q_d^2 and hence potentially stronger running effects.

We identified several short-baseline experiments that place stringent constraints on the running: NOMAD [63,76] (bounds from CHORUS [77,78] are qualitatively comparable and so are the associated neutrino energies), CHARM-II [79], ICARUS [80], and NuTeV [67,81]; see Table I for their reference values of energies and momentum transfers. All these experiments measured neutrino beams that were primarily composed of muon neutrinos.[8] Electron neutrino appearance was severely constrained by all of them, while NOMAD and NuTeV also constrained anomalous $\nu_\mu \to \nu_\tau$ transitions. NuTeV, due to its non-negligible beam ν_e component, also managed to put a bound on $\nu_e \to \nu_\tau$ appearance. Concrete upper bounds for each appearance channel are listed in Table I. While NOMAD and NuTeV provide the most stringent bounds on appearance probabilities, it is important to include constraints obtained with different neutrino energies and thus the information provided by the other experiments is invaluable.

The right-hand panel of Fig. 3 depicts the biprobability plot for T2K (red points) and Nova (blue points) for the NO, assuming the lightest neutrino mass to be $m_1 = 0.05$ eV. As before, we revisit the same 30,000 model points depicted in the left-hand panel of Fig. 3, but here only keep those points that satisfy the constraints from the short-baseline experiments listed in Table I. Models associated with a very large effect on Nova and T2K appearance channels were also very likely to violate the short-baseline constraints. From a model-parameter perspective, zero-baseline constraints disfavor regions of the parameter space with $\mathcal{O}(1)$ Yukawa couplings when the neutrino masses are large. Ultimately, the new-physics effects consistent with short-baseline constraints are, at T2K and Nova, "perturbations" on standard oscillations. Notice, however, that significant deviations are still allowed; a significant fraction of the points in the right-hand panel of Fig. 3 lies outside the standard (no-running) 1σ-allowed ranges for T2K and Nova.

RG-running effects depend strongly on the active neutrino masses and tend to be largest when these are quasidegenerate. The left panel of Fig. 4 depicts the biprobability plot at T2K (red points) and Nova (blue points) for the NO, this time assuming the lightest neutrino mass to be $m_1 = 0.01$ eV, for 30,000 values of the model parameters. The right panel of Fig. 4 depicts the subset of points that satisfy the short-baseline constraints. Comparing Fig. 3 with Fig. 4, we see that the region of the biprobability plots accessible to the new physics is larger for quasidegenerate neutrinos, $m_1 = 0.05$ eV, when compared to the more hierarchical case, $m_1 = 0.01$ eV.

[8] As a simplifying assumption, we treat all beam neutrinos as if they were the product of pion decay in flight.

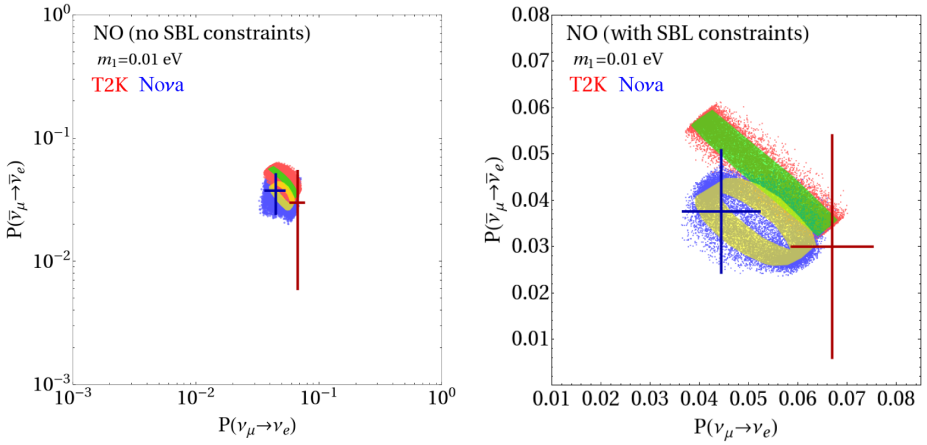

FIG. 4. Same as Fig. 3 for the case of NO and $m_1 = 0.01$ eV.

Similarly, Fig. 5 depicts the RG effects on T2K and Nova for the IO and $m_3 = 0.01$ eV (the lightest neutrino mass). Here, even for a relatively light lightest neutrino mass, running effects are comparable to the NO scenario with larger neutrino masses, discussed earlier. Thus, for the same mass of the lightest neutrino, the RG effects are larger for IO relative to NO. As expected, the short-baseline constraints are very relevant here as well.

While Figs. 3–5 illustrate the general overall reach of the RG effect on the appearance channels, it is also useful to understand how RG effects impact oscillations for a specific fixed values of the oscillation parameters at Q_p^2. Figure 6 depicts the impact of RG running at T2K (left) and Nova (right), including constraints from the short-baseline experiments, for different fixed values of all oscillation parameters at Q_p^2. Modulo rare outliers, the relative new-physics effect, that is, the distance from respective black dot, is of order 10%. Moreover, the RG effects tend to modify neutrino and antineutrino appearance by similar amounts, while extra contributions to the CP asymmetry are somewhat suppressed. This can be understood from Eq. (III.19), in particular, the $\cot(\Delta_{31}/2)$ term that is almost vanishing for T2K at the peak of the energy spectrum. Similar shifts due to new physics on both neutrino and antineutrino appearances can be mimicked by changing the value of $\sin^2\theta_{23}$. Therefore, one possible experimental outcome of this scenario could be an apparent inconsistency between the $\sin^2\theta_{23}$ values obtained from the disappearance channel and the $\sin^2\theta_{23}$ from the appearance channel.

Since RG effects modify oscillation probabilities at T2K and Nova in slightly different ways, it is interesting to investigate whether they could explain the mild tension between the current T2K and Nova electron (anti)neutrino appearance datasets. To do this, we designed a toy χ^2 using the aforementioned T2K and Nova data points in the biprobability plane,

$$\chi^2 = \sum_X \sum_{i=\nu,\bar{\nu}} \left(\frac{D_i^X - T_i^X}{\sigma_i^X} \right)^2, \tag{5.1}$$

where X denotes T2K or Nova, D_i^X (T_i^X) is the measured (predicted) value of the probability at the experiment X and

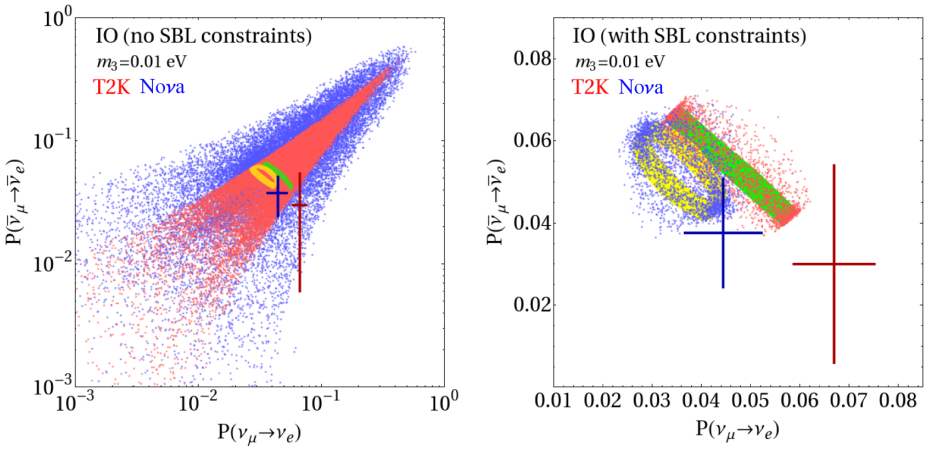

FIG. 5. Same as Fig. 3 for the case of IO and $m_3 = 0.01$ eV.

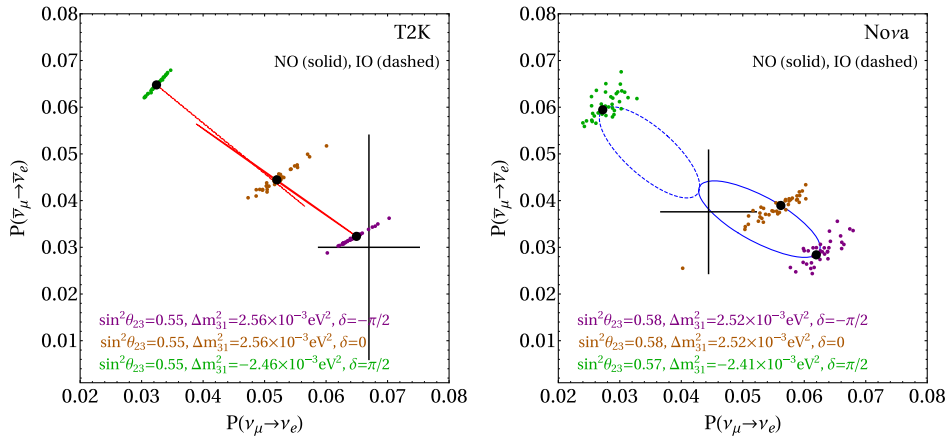

FIG. 6. Biprobability plots—T2K on the right, Nova on the left—for both mass orderings and the lightest mass set to 0.05 eV. The dots indicate the three benchmark points in the standard case. These lie on their respective ellipses, obtained by fixing θ_{23} and Δm^2_{31} and varying $\delta \in [0, 2\pi]$. The colored points represent different choices of the new-physics parameters and are indicative of typical RG effects once zero-baseline constraints are included.

run mode $i = \nu, \bar{\nu}$, and σ_i^X is the error bar read from the plot. Out of the 30,000 generated model points, we found $\mathcal{O}(10)$ parameter points for NO and $m_1 = 0.05$ eV, which satisfy the short-baseline constraints and provide a slightly better fit to data, though none are statistically significant. Since the combined fit to T2K and Nova data leads to a small preference for the inverted ordering [75], it is harder to improve the fit in the IO case. Out of the 30,000 generated model points for the IO, we found no points that provide a better fit to data compared to standard oscillations.

To further illustrate the RG effects, especially their dependence on the neutrino energy, we depict the electron (anti)neutrino appearance probabilities at T2K (top) and Nova (bottom), in Fig. 7, for NO and $m_1 = 0.05$ eV. Red and green curves correspond to the oscillation probabilities for neutrinos and antineutrinos, respectively, at T2K, while curves in shades of blue are constructed by adopting the Nova far detector baseline. The vertical bands indicate the peak of the energy spectrum for each of the two experiments. The left-hand panels depict the oscillation probabilities for the benchmark point in our scan (denoted by BP1),[9] which best fits T2K and Nova data (solid), compared with the case where the mixing parameters are the same at Q_p^2 but there are no running effects (dashed). The lower part of each figure depicts the relative difference between these two hypotheses. While the differences are small, the relative differences are of order 10%, growing as the neutrino energy grows due to larger accessible values of the momentum transfer. The right-hand panels of Fig. 7 depict the case of a different benchmark point, denoted BP2. BP2 is excluded by the short-baseline data. Nonetheless, it serves to illustrate the possible impact of RG effects on oscillation experiments and to highlight the importance of the short-baseline experiments.

Figure 8 depicts the RG evolution of the relevant mixing parameters for both benchmark points BP1 and BP2. The left-hand panel depicts the values of the different parameters as a function of $\sqrt{Q^2}$, while the right-hand panel depicts the ratio between each parameter at Q^2 relative to its value at Q_p^2. For BP1 (solid), RG evolution yields few percent-level changes in the values of oscillation parameters. Running effects are more pronounced in the case of BP2 (dashed). The strongest effects are in running of θ_{12}, which is very strongly impacted by RG effects. This large variation in θ_{12} disturbs all flavor transitions and induces sizable zero-baseline effects as $U(Q_d^2)U^\dagger(Q_p^2)$ strongly deviates from unity. Hence, these points in model space are strongly constrained by both short- and long-baseline experiments. In general, we find that, when strong RG evolution effects are present, they typically first appear in θ_{12}. It is well known [32] that the variation of θ_{12} relative to the other mixing angles θ_{13} and θ_{23} is enhanced by the ratio between atmospheric and solar mass-squared differences: $|\Delta\theta_{12}/\Delta\theta_{13}|, |\Delta\theta_{12}/\Delta\theta_{23}| \propto |\Delta m^2_{31}/\Delta m^2_{21}|$.[10]

[9]For completeness and reproducibility, we provide the two benchmark points discussed here. They can be obtained by using Eq. (IV.7) with the parameters $(\delta, \tilde{\alpha}, \tilde{\beta}, \xi_1, \xi_2, \xi_3, \theta_{23}, \Delta m^2_{31}/10^{-3}\ \text{eV}^2)$ equal to (3.71,1.57,2.37,3.45,1.51,3.00,0.88,2.437) for BP1 and (1.18,0.24,1.64,5.48,2.076,1.85,0.86,2.525) for BP2 (all angles and phases are in radians).

[10]In our phenomenological discussions of RG-running effects at T2K and Nova, we did not highlight the fact that θ_{12}-running effects are largest. The reason is that long-baseline experiments (and all other "high-energy" experiments, including measurements of the atmospheric neutrino flux) have limited ability to constrain the solar oscillation parameters, since, for the typical energies associated with these setups, $E/\Delta m^2$ is much larger than the relevant baselines. While higher precision and more statistics are expected at DUNE and Hyper-Kamiokande, these will also have only limited ability to independently measure θ_{12}.

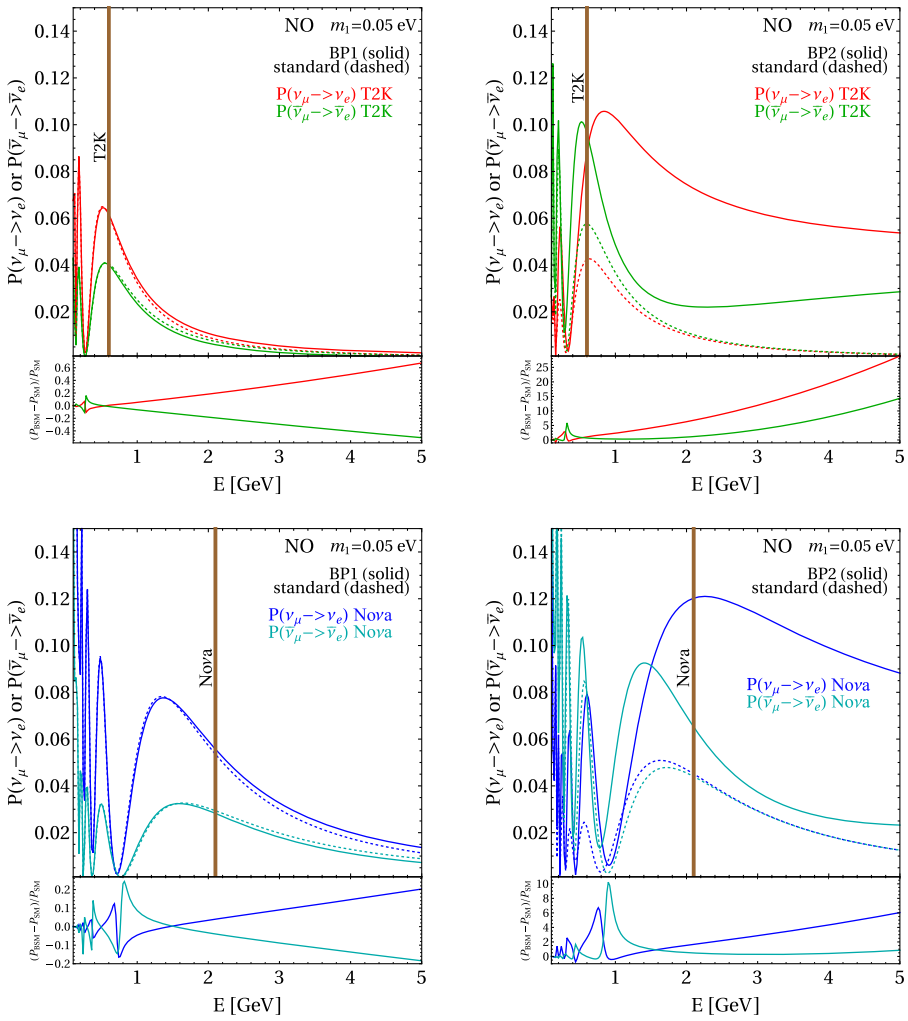

FIG. 7. Oscillation probabilities as a function of the neutrino energy at T2K (upper) and Noνa (lower) including (solid) RG-running effects or not (dashed). In the left-hand panels, the new-physics parameters are the ones that provide the best fit we found for the combined T2K and Noνa data. In the right-hand panels, the new-physics parameters are strongly excluded by short-baseline constraints. We assume the NO and the lightest neutrino mass is set to 0.05 eV. The vertical lines indicate the neutrino energies where the T2K and Noνa spectra are largest. The bottom portion of each panel depicts the relative differences between oscillation probabilities with and without RG-running effects.

Finally, since RG effects on short-baseline experiments can be sizable, one may be tempted to search for explanations to the LSND [5] and/or MiniBooNE [7,8] anomalies using this framework. In particular, we found plenty of points in model space with zero-baseline appearance probability $P_{\nu_\mu\to\nu_e} \simeq 10^{-3}$ at around $E_\nu \simeq 0.4$ GeV, hence qualitatively in agreement with the oscillation interpretation of the MiniBooNE data. However, once constraints from NOMAD and NuTeV are imposed, such points are ruled out. This is mostly because RG effects are stronger at larger neutrino energies. We will explore the short-baseline phenomenology of this framework and variations thereof in more detail in an upcoming manuscript.

B. Ultrahigh-energy neutrinos from the cosmos

Neutrino oscillation experiments are not the only way to search for the RG running of neutrino mixing parameters. In particular, RG effects grow with Q^2 and the IceCube experiment has detected neutrinos from extragalactic astrophysical sources with laboratory energies up to the PeV scale. This corresponds to $\sqrt{Q_d^2} \simeq 10^3$ GeV, far above the corresponding values accessible to terrestrial experiments (see Table I). Here we argue that precise measurements of the flavor composition of ultrahigh-energy (UHE) neutrinos at IceCube are also sensitive to the new-physics effects discussed here.

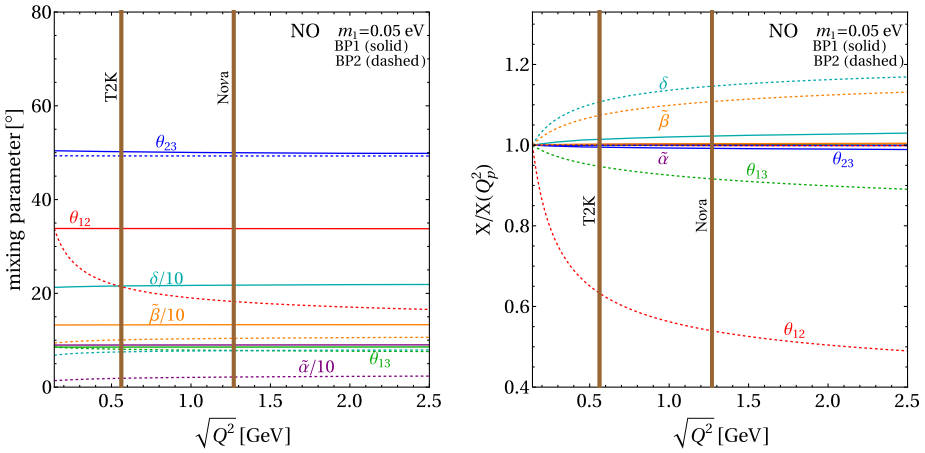

FIG. 8. Left: RG evolution of the mixing parameters for the two new-physics parameter points in Fig. 7. The solid (dashed) lines are for the best-fit (strongly excluded) point. The vertical lines denote the peak value of $\sqrt{Q^2}$ at T2K and Noνa. Right: RG evolution of the mixing parameters, normalized by the respective values at Q_p^2.

In Sec. V A, we focused on RG effects for $m_\pi^2 \leq Q_d^2 \lesssim (16)^2$ GeV^2 and concluded that new-physics effects were a perturbation over the standard expectation, particularly due to constraints from short-baseline experiments. Here, we will modify the RG-running conditions and assume that the RG effects only take place for $\sqrt{Q^2} \gg 16$ GeV; i.e., the new degrees of freedom have masses on the order of tens of GeV. This assumption leads to no observable effects at Solar System neutrino experiments but allows for potentially strong effects on measurements of the flavor composition of IceCube's UHE neutrinos. For the purpose of our calculations, we postulate that running starts at $\sqrt{Q_p^2} = 16$ GeV and the values of all the parameters at $\sqrt{Q^2} = 16$ GeV are consistent with existing constraints from oscillation experiments. It is important to note that UHE neutrinos are produced, for the most part, in the decays of pions, muons, or perhaps neutrons so Q_p^2 is usually around or below m_π^2, independent from the neutrino energy. Since the running only starts at the mass scale of new particles, calculating the running from m_π^2 to Q_d^2 is equivalent to setting the production Q_p^2 to the mass scale of new particles. As far as detection at IceCube is concerned, we fix $\sqrt{Q_d^2} = 10^3$ GeV, for simplicity.

The IceCube Collaboration has released results [82,83] on the flavor composition of astrophysical neutrinos, an observable that is also one of the pillars of the forthcoming IceCube-Gen2 upgrade [84–86]. The initial flavor composition (ν_e:ν_μ:ν_τ) of $\mathcal{O}$ (PeV) neutrinos (note that, here, we do not distinguish between neutrinos and antineutrinos) from astrophysical neutrino sources is uncertain due to our poor knowledge of the nature of these sources and the mechanism behind neutrino production. We will consider several hypotheses. If the neutrinos are predominantly produced in the decays of high-energy pions and in the decays of the pion-daughter muons, the flavor ratios at production would be (1:2:0) [87,88]. If, on the other hand, muons from the pion decays lose most of the their energy before decaying (e.g., due to interactions in a dense medium [89]), their decay products are not very energetic and the initial flavor composition would be (0:1:0) [90,91]. If, on the other hand, neutron decays are the dominant source of UHE neutrinos, only electron antineutrinos would be produced at the source: (1:0:0) [92]. It turns out that neutron decays as the dominant source of UHE neutrinos are disfavored at around the 68% CL by IceCube data [82,83]. For completeness, one could also consider a pure tau neutrino initial flavor composition (0:0:1) [93–95] even if this is not expected to occur in any known astrophysical environment.

Once produced, the propagation of neutrinos to Earth is subject to neutrino oscillations. Given the very long baselines, it is safe to treat these neutrinos are incoherent superpositions of mass eigenstates and the oscillation probabilities at Earth are baseline independent. In the standard three-neutrino paradigm, the probability of producing an astrophysical neutrino of flavor α and detecting it with flavor β, $\alpha, \beta = e, \mu, \tau$, is given by

$$P_{\nu_\alpha \to \nu_\beta} = P_{\nu_\beta \to \nu_\alpha} = \delta_{\alpha\beta} - 2\sum_{k>j} \mathrm{Re}[U_{\alpha k}^* U_{\beta k} U_{\alpha j} U_{\beta j}^*] = \sum_{j=1}^{n} |U_{\alpha j}|^2 |U_{\beta j}|^2. \quad (5.2)$$

In the presence of mixing-matrix running, these probabilities are [96]

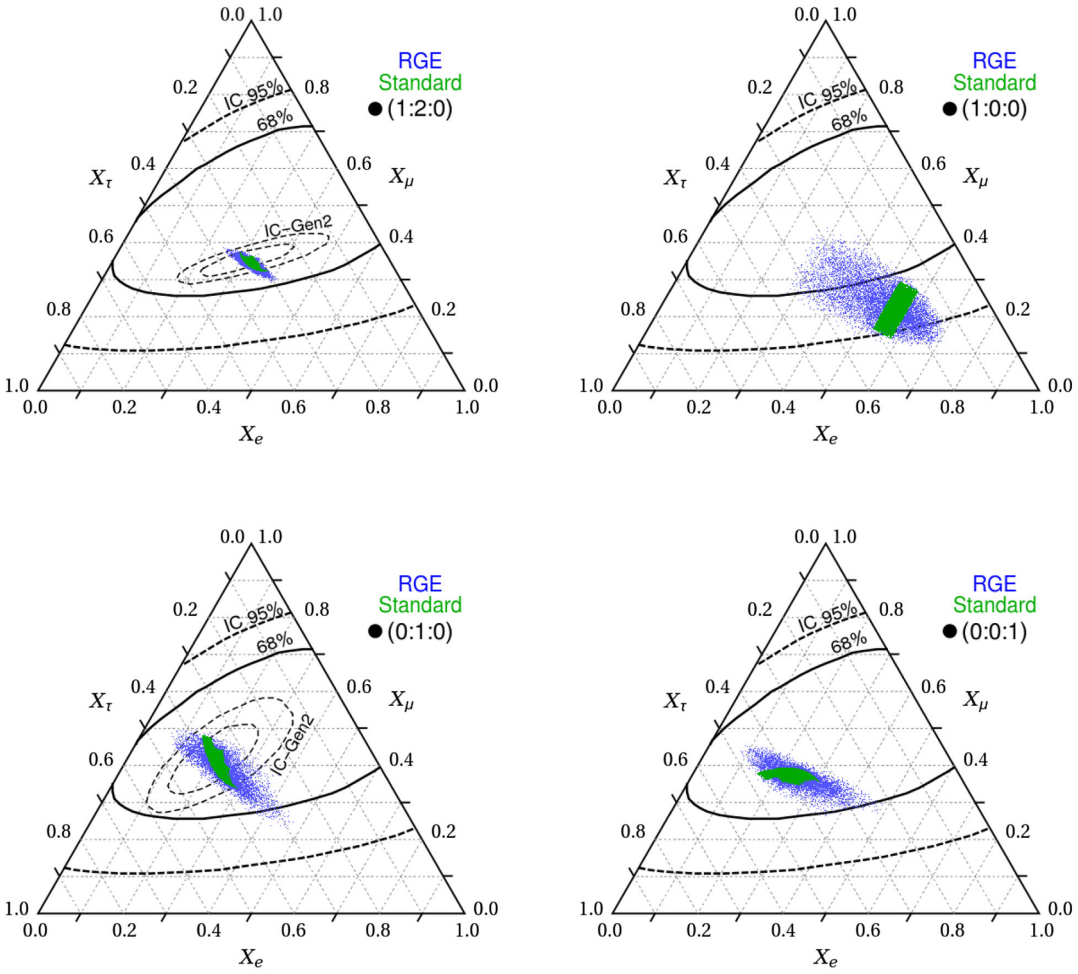

FIG. 9. The relative flavor composition of UHE astrophysical neutrinos at Earth for different choices of the relative flavor composition at the source. The green region corresponds to expectations from standard three-neutrino oscillations, while the blue scatter points represent the potential effects of mixing-matrix running. Present limits from IceCube are shown as thick dashed (68% CL) and thick solid (95% CL) lines. For pion-decay and damped-muon sources (left top and left bottom, respectively), we also show IceCube Gen-2 projections as thin dashed lines (68% and 95% CL). See text for details.

$$P_{\nu_\alpha \to \nu_\beta} = \sum_{j=1}^{3} |U_{\alpha j}(Q_p^2)|^2 |U_{\beta j}(Q_d^2)|^2, \tag{5.3}$$

where we again stress that mixing-matrix elements evaluated at the Q_p^2 and Q_d^2 scales are potentially different. The expected flavor composition at the surface of Earth is

$$X_\beta = \sum_\alpha P_{\nu_\alpha \to \nu_\beta} X_\alpha^{\text{prod}}, \tag{5.4}$$

where X_α^{prod} is the fraction of neutrinos of flavor α at production.

Figure 9 depicts the flavor compositions in the ternary plots that are often employed for this type of study [97,98]. Each panel corresponds to one of the production scenarios discussed above. Green regions indicate the accessible range in the flavor triangle for standard neutrino oscillations, whereas blue scatter points represent different scenarios with RG effects (RGE in the figure) included. The parameter-scan strategy is similar to the one discussed in Sec. V A for both the standard scenario and the different new-physics models. In all panels, the new-physics effects increase the accessible region of the flavor triangle when compared to the standard case due to the mismatch between production and detection mixing-matrix elements. The most striking effect can be seen in the upper right-hand panel, associated with (1:0:0) (neutron decay source) at production. As we discussed, while this type of production is disfavored by present data in the absence of new physics, the situation is different once RG-running effects are included; as can be seen in the figure, there are plenty of blue points safely located inside the 68% CL region.

For the preferred (1:2:0) and (0:1:0) scenarios, we also depict, in addition to present constraints, the future projections of IceCube-Gen2 [85]. The region defined by

the blue scatter points exceeds those regions significantly. Hence, as the efforts in the field of neutrino astrophysics lead to the discovery of point sources and illuminate the neutrino-production mechanism, it will be possible to use the flavor-composition observable to probe the presence of RG induced new-physics effects with some precision. Finally, we also consider the more general production scenario in which the flavor composition is a generic mixture of electron and muon neutrinos. Figure 10 depicts the flavor triangles for initial flavor ratios given by $(x:(1-x):0)$, $x \in [0,1]$, where we scan over all possible values of $x \in [0,1]$. As in Fig. 9, it is clearly visible that mixing-matrix running may lead to strong effects on the flavor composition at Earth. We can repeat this exercise for a most general source of the type $(x(1-y):(1-x)(1-y):y)$, $x, y \in [0,1]$. In this case, we also find that running effects can land well outside the region one can access in the context of the standard scenario.

We conclude this subsection by summarizing the main effects induced by the running of the mixing matrix:

(i) Even if the running of the mixing matrix starts at energy scales higher than those accessible to Solar System neutrino experiments, the impact on the flavor composition of UHE neutrinos can be quite large.

(ii) The main effect of the running is to enlarge the set of allowed values for the flavor ratios at IceCube, for all production mechanisms. A signature of this scenario is the measurement of a flavor composition of the UHE neutrino flux that is inconsistent with expectations from standard three-neutrino oscillations.

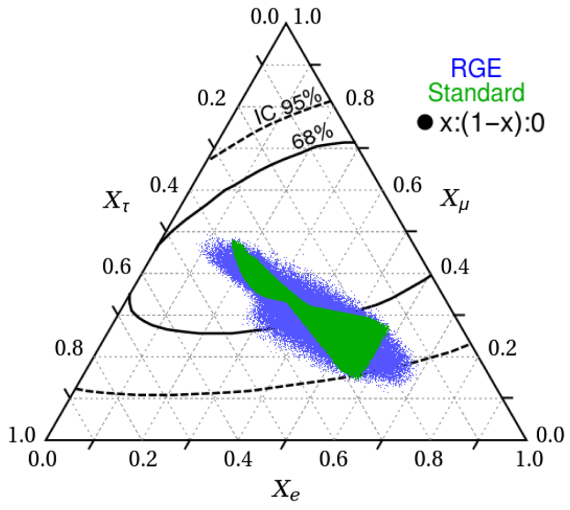

FIG. 10. Same as Fig. 9, for all possible flavor compositions ($x \in [0,1]$), assuming the sources can only produce electron and muon neutrinos.

VI. CONCLUSIONS

We considered, within the context of simple, ultraviolet-complete models of neutrino masses, the effects of scale-dependent lepton mixing parameters at neutrino oscillation experiments. In this framework, the mixing matrix at production and detection may be different, leading to rich and novel phenomenological consequences. We identified several robust experimental signatures of this framework, including

(i) apparent mismatches between θ_{13} measurements at reactor and beam experiments as well as apparent mismatches between θ_{23} measurements in ν_μ disappearance and ν_e appearance channels (this would be the smoking gun signature of the framework proposed in this paper),

(ii) new sources of CP-invariance violation,

(iii) zero-baseline flavor transitions $\nu_\mu \to \nu_\tau$, $\nu_\mu \to \nu_e$ and $\nu_e \to \nu_\tau$,

(iv) apparent CPT-invariance violation in the form $P(\nu_\alpha \to \nu_\alpha) \neq P(\bar{\nu}_\alpha \to \bar{\nu}_\alpha)$ for $\alpha = e, \mu, \tau$.

Taking current experimental constraints from short-baseline experiments into account, we showed that the renormalization-group evolution of the mixing parameters can induce observable effects at T2K, Noνa, and future long-baseline neutrino experiments. As a complementary probe to short- and long-baseline experiments, we also scrutinized effects at neutrino telescopes, in particular, those related to the flavor composition of ultrahigh-energy neutrinos.

Observable effects of RG running of the leptonic mixing matrix are a potential consequence of new, relatively light degrees of freedom and new neutrino interactions. As we demonstrated, the new interactions may be restricted, mostly, to the neutrino sector and hence are difficult to constrain outside of experiments that involve flavor-resolved neutrino scattering. The effects discussed here are qualitatively different from the more familiar nonstandard neutral-current-like neutrino interactions, which often manifest themselves via modified matter effects or new interactions that impact neutrino production or detection. The latter, in particular, may also be described using different leptonic mixing matrices at neutrino production relative to neutrino detection, but do not share the scale dependency of the RG-running effects discussed here. New, light degrees of freedom can also be directly produced in neutrino scattering. These effects are complementary to what we are discussing here and have been explored, rather recently, in the literature.

ACKNOWLEDGMENTS

We thank Bill Bardeen and Joachim Kopp for useful discussions. This work was supported in part by the US

Department of Energy (DOE) Award No. de-sc0010143 and in part by the NSF Grant No. PHY-1630782. Fermilab is managed by Fermi Research Alliance, LLC (FRA), acting under Contract No. DE-AC02-07CH11359. This project has received support from the European Union's Horizon 2020 research and innovation program under the Marie Skłodowska-Curie Grant Agreement No. 860881-HIDDeN.

[1] Y. Fukuda *et al.* (Super-Kamiokande Collaboration), Evidence for Oscillation of Atmospheric Neutrinos, Phys. Rev. Lett. **81**, 1562 (1998).
[2] Q. R. Ahmad *et al.* (SNO Collaboration), Direct Evidence for Neutrino Flavor Transformation from Neutral Current Interactions in the Sudbury Neutrino Observatory, Phys. Rev. Lett. **89**, 011301 (2002).
[3] B. Abi *et al.* (DUNE Collaboration), Deep Underground Neutrino Experiment (DUNE), far detector technical design report, volume I introduction to DUNE, J. Instrum. **15**, T08008 (2020).
[4] K. Abe *et al.* (Hyper-Kamiokande Collaboration), Hyper-Kamiokande design report, arXiv:1805.04163.
[5] C. Athanassopoulos *et al.* (LSND Collaboration), Evidence for $\bar{\nu}_\mu \to \bar{\nu}_e$ Oscillations from the LSND Experiment at Los Alamos Meson Physics Facility, Phys. Rev. Lett. **77**, 3082 (1996).
[6] A. A. Aguilar-Arevalo *et al.* (MiniBooNE Collaboration), Event Excess in the MiniBooNE Search for $\bar{\nu}_\mu \to \bar{\nu}_e$ Oscillations, Phys. Rev. Lett. **105**, 181801 (2010).
[7] A. A. Aguilar-Arevalo *et al.* (MiniBooNE Collaboration), Significant Excess of Electronlike Events in the MiniBooNE Short-Baseline Neutrino Experiment, Phys. Rev. Lett. **121**, 221801 (2018).
[8] A. A. Aguilar-Arevalo *et al.* (MiniBooNE Collaboration), Updated MiniBooNE neutrino oscillation results with increased data and new background studies, Phys. Rev. D **103**, 052002 (2021).
[9] T. A. Mueller *et al.*, Improved predictions of reactor antineutrino spectra, Phys. Rev. C **83**, 054615 (2011).
[10] P. Huber, On the determination of anti-neutrino spectra from nuclear reactors, Phys. Rev. C **84**, 024617 (2011); **85**, 029901(E) (2012).
[11] S. Davidson, C. Pena-Garay, N. Rius, and A. Santamaria, Present and future bounds on nonstandard neutrino interactions, J. High Energy Phys. 03 (2003) 011.
[12] A. Ibarra, E. Masso, and J. Redondo, Systematic approach to gauge-invariant relations between lepton flavor violating processes, Nucl. Phys. **B715**, 523 (2005).
[13] M. B. Gavela, D. Hernandez, T. Ota, and W. Winter, Large gauge invariant non-standard neutrino interactions, Phys. Rev. D **79**, 013007 (2009).
[14] C. Biggio, M. Blennow, and E. Fernandez-Martinez, Loop bounds on non-standard neutrino interactions, J. High Energy Phys. 03 (2009) 139.
[15] S. Davidson and M. Gorbahn, Charged lepton flavor change and nonstandard neutrino interactions, Phys. Rev. D **101**, 015010 (2020).
[16] Y. Farzan and I. M. Shoemaker, Lepton flavor violating nonstandard interactions via light mediators, J. High Energy Phys. 07 (2016) 033.
[17] Y. Farzan and J. Heeck, Neutrinophilic nonstandard interactions, Phys. Rev. D **94**, 053010 (2016).
[18] K. S. Babu, A. Friedland, P. A. N. Machado, and I. Mocioiu, Flavor gauge models below the Fermi scale, J. High Energy Phys. 12 (2017) 096.
[19] Y. Farzan and M. Tórtola, Neutrino oscillations and nonstandard interactions, Front. Phys. **6**, 10 (2018).
[20] J. M. Berryman, A. de Gouvêa, K. J. Kelly, and Y. Zhang, Lepton-number-charged scalars and neutrino beamstrahlung, Phys. Rev. D **97**, 075030 (2018).
[21] V. Brdar, W. Rodejohann, and X.-J. Xu, Producing a new fermion in coherent elastic neutrino-nucleus scattering: From neutrino mass to dark matter, J. High Energy Phys. 12 (2018) 024.
[22] W.-F. Chang and J. Liao, Constraints on light singlet fermion interactions from coherent elastic neutrino-nucleus scattering, Phys. Rev. D **102**, 075004 (2020).
[23] N. Hurtado, H. Mir, I. M. Shoemaker, E. Welch, and J. Wyenberg, Dark matter-neutrino interconversion at COHERENT, direct detection, and the early Universe, Phys. Rev. D **102**, 015006 (2020).
[24] W. Abdallah, R. Gandhi, and S. Roy, Understanding the MiniBooNE and the muon and electron $g-2$ anomalies with a light Z' and a second Higgs doublet, J. High Energy Phys. 12 (2020) 188.
[25] V. Brdar, O. Fischer, and A. Y. Smirnov, Model-independent bounds on the nonoscillatory explanations of the MiniBooNE excess, Phys. Rev. D **103**, 075008 (2021).
[26] K. S. Babu, C. N. Leung, and J. T. Pantaleone, Renormalization of the neutrino mass operator, Phys. Lett. B **319**, 191 (1993).
[27] P. H. Chankowski and Z. Pluciennik, Renormalization group equations for seesaw neutrino masses, Phys. Lett. B **316**, 312 (1993).
[28] S. Antusch, M. Drees, J. Kersten, M. Lindner, and M. Ratz, Neutrino mass operator renormalization revisited, Phys. Lett. B **519**, 238 (2001).
[29] J. A. Casas, J. R. Espinosa, A. Ibarra, and I. Navarro, General RG equations for physical neutrino parameters and their phenomenological implications, Nucl. Phys. **B573**, 652 (2000).
[30] K. R. S. Balaji, A. S. Dighe, R. N. Mohapatra, and M. K. Parida, Radiative magnification of neutrino mixings and a natural explanation of the neutrino anomalies, Phys. Lett. B **481**, 33 (2000).

[31] S. Antusch, J. Kersten, M. Lindner, and M. Ratz, Running neutrino masses, mixings and *CP* phases: Analytical results and phenomenological consequences, Nucl. Phys. **B674**, 401 (2003).
[32] S. Antusch, J. Kersten, M. Lindner, M. Ratz, and M. A. Schmidt, Running neutrino mass parameters in see-saw scenarios, J. High Energy Phys. 03 (2005) 024.
[33] S. Goswami, S. T. Petcov, S. Ray, and W. Rodejohann, Large—U(e3)—and Tri-bimaximal mixing, Phys. Rev. D **80**, 053013 (2009).
[34] P. Abreu *et al.* (DELPHI Collaboration), m(b) at M(Z), Phys. Lett. B **418**, 430 (1998).
[35] A. Brandenburg, P. N. Burrows, D. Muller, N. Oishi, and P. Uwer, Measurement of the running b quark mass using e + e-− > b anti-b g events, Phys. Lett. B **468**, 168 (1999).
[36] G. Abbiendi *et al.* (OPAL Collaboration), Determination of the b quark mass at the Z mass scale, Eur. Phys. J. C **21**, 411 (2001).
[37] J. Abdallah *et al.* (DELPHI Collaboration), Determination of the b quark mass at the M(Z) scale with the DELPHI detector at LEP, Eur. Phys. J. C **46**, 569 (2006).
[38] U. Langenfeld, S. Moch, and P. Uwer, Measuring the running top-quark mass, Phys. Rev. D **80**, 054009 (2009).
[39] A. M. Sirunyan *et al.* (CMS Collaboration), Running of the top quark mass from proton-proton collisions at $\sqrt{s} = 13$ TeV, Phys. Lett. B **803**, 135263 (2020).
[40] K. S. Babu, Renormalization group analysis of the Kobayashi-Maskawa matrix, Z. Phys. C **35**, 69 (1987).
[41] I. P. Volobuev, Quantum field-theoretical description of neutrino and neutral kaon oscillations, Int. J. Mod. Phys. A **33**, 1850075 (2018).
[42] Y. Grossman, Nonstandard neutrino interactions and neutrino oscillation experiments, Phys. Lett. B **359**, 141 (1995).
[43] A. Falkowski, M. González-Alonso, and Z. Tabrizi, Reactor neutrino oscillations as constraints on effective field theory, J. High Energy Phys. 05 (2019) 173.
[44] C. O. Anoka, Anomaly mediated supersymmetry breaking and nonstandard neutrino oscillations, Ph.D. thesis, Oklahoma State University, 2005.
[45] C. Jarlskog, Commutator of the Quark Mass Matrices in the Standard Electroweak Model and a Measure of Maximal *CP* Violation, Phys. Rev. Lett. **55**, 1039 (1985).
[46] C. Jarlskog, A basis independent formulation of the connection between quark mass matrices, *CP* violation and experiment, Z. Phys. C **29**, 491 (1985).
[47] K. Abe *et al.* (T2K Collaboration), Search for Electron Antineutrino Appearance in a Long-Baseline Muon Antineutrino Beam, Phys. Rev. Lett. **124**, 161802 (2020).
[48] M. A. Acero *et al.* (NOνA Collaboration), First Measurement of Neutrino Oscillation Parameters Using Neutrinos and Antineutrinos by NOνA, Phys. Rev. Lett. **123**, 151803 (2019).
[49] E. Ma, Verifiable radiative seesaw mechanism of neutrino mass and dark matter, Phys. Rev. D **73**, 077301 (2006).
[50] Y. Chikashige, R. N. Mohapatra, and R. D. Peccei, Are there real Goldstone bosons associated with broken lepton number?, Phys. Lett. **98B**, 265 (1981).
[51] P. Minkowski, $\mu \to e\gamma$ at a rate of one out of 10^9 muon decays?, Phys. Lett. **67B**, 421 (1977).
[52] M. Gell-Mann, P. Ramond, and R. Slansky, Complex spinors and unified theories, Conf. Proc. C **790927**, 315 (1979).
[53] T. Yanagida, Horizontal gauge symmetry and masses of neutrinos, Conf. Proc. C **7902131**, 95 (1979).
[54] S. L. Glashow, The future of elementary particle physics, NATO Sci. Ser. B **61**, 687 (1980).
[55] R. N. Mohapatra and G. Senjanovic, Neutrino Mass and Spontaneous Parity Nonconservation, Phys. Rev. Lett. **44**, 912 (1980).
[56] J. Schechter and J. W. F. Valle, Neutrino masses in $SU(2) \times U(1)$ theories, Phys. Rev. D **22**, 2227 (1980).
[57] J. A. Casas and A. Ibarra, Oscillating neutrinos and $\mu \to e, \gamma$, Nucl. Phys. **B618**, 171 (2001).
[58] K. Abe *et al.* (T2K Collaboration), Search for *CP* Violation in Neutrino and Antineutrino Oscillations by the T2K Experiment with 2.2×10^{21} Protons on Target, Phys. Rev. Lett. **121**, 171802 (2018).
[59] K. Abe *et al.* (T2K Collaboration), Constraint on the matter–antimatter symmetry-violating phase in neutrino oscillations, Nature (London) **580**, 339 (2020); **583**, E16 (2020).
[60] P. Adamson *et al.* (NOνA Collaboration), Constraints on Oscillation Parameters from ν_e Appearance and ν_μ Disappearance in NOνA, Phys. Rev. Lett. **118**, 231801 (2017).
[61] M. A. Acero *et al.* (NOνA Collaboration), New constraints on oscillation parameters from ν_e appearance and ν_μ disappearance in the NOνA experiment, Phys. Rev. D **98**, 032012 (2018).
[62] F. Vannucci, The NOMAD experiment at CERN, Adv. High Energy Phys. **2014**, 1 (2014).
[63] P. Astier *et al.* (NOMAD Collaboration), Final NOMAD results on $\nu_\mu \to \nu_\tau$ and $\nu_e \to \nu_\tau$ oscillations including a new search for ν_τ appearance using hadronic τ decays, Nucl. Phys. **B611**, 3 (2001).
[64] P. Astier *et al.* (NOMAD Collaboration), Search for $\nu_\mu \to \nu_e$ oscillations in the NOMAD experiment, Phys. Lett. B **570**, 19 (2003).
[65] M. Antonello *et al.*, Experimental search for the "LSND anomaly" with the ICARUS detector in the CNGS neutrino beam, Eur. Phys. J. C **73**, 2345 (2013).
[66] P. Vilain *et al.* (CHARM II Collaboration), Precision measurement of electroweak parameters from the scattering of muon-neutrinos on electrons, Phys. Lett. B **335**, 246 (1994).
[67] D. Naples *et al.* (CCFR/NuTeV Collaboration), A high statistics search for $\nu_e(\bar{\nu}_e) \to \nu_\tau(\bar{\nu}_\tau)$ oscillations, Phys. Rev. D **59**, 031101 (1998).
[68] S. Avvakumov *et al.* (NuTeV Collaboration), A Search for $\nu_\mu \to \nu_e$ and $\bar{\nu}_\mu \to \bar{\nu}_e$ Oscillations at NuTeV, Phys. Rev. Lett. **89**, 011804 (2002).
[69] M. G. Aartsen *et al.* (IceCube Collaboration), Evidence for high-energy extraterrestrial neutrinos at the IceCube detector, Science **342**, 1242856 (2013).
[70] M. G. Aartsen *et al.* (IceCube Collaboration), Observation of High-Energy Astrophysical Neutrinos in Three Years of IceCube Data, Phys. Rev. Lett. **113**, 101101 (2014).
[71] R. Abbasi *et al.* (IceCube Collaboration), The IceCube high-energy starting event sample: Description and flux characterization with 7.5 years of data, Phys. Rev. D **104**, 022002 (2021).

[72] I. Esteban, M. C. Gonzalez-Garcia, M. Maltoni, T. Schwetz, and A. Zhou, The fate of hints: Updated global analysis of three-flavor neutrino oscillations, J. High Energy Phys. 09 (2020) 178.
[73] N. Aghanim *et al.* (Planck Collaboration), Planck 2018 results. VI. Cosmological parameters, Astron. Astrophys. **641**, A6 (2020).
[74] P. A. Zyla *et al.* (Particle Data Group), Review of particle physics, Prog. Theor. Exp. Phys. **2020**, 083C01 (2020).
[75] K. J. Kelly, P. A. N. Machado, S. J. Parke, Y. F. Perez-Gonzalez, and R. Z. Funchal, Neutrino mass ordering in light of recent data, Phys. Rev. D **103**, 013004 (2021).
[76] P. Astier *et al.* (NOMAD Collaboration), Search for $\nu_\mu \to \nu_e$ oscillations in the NOMAD experiment, Phys. Lett. B **570**, 19 (2003).
[77] E. Eskut *et al.* (CHORUS Collaboration), The CHORUS experiment to search for $\nu_\mu \to \nu_\tau$ oscillation, Nucl. Instrum. Methods Phys. Res., Sect. A **401**, 7 (1997).
[78] E. Eskut *et al.* (CHORUS Collaboration), New results from a search for $\nu_\mu \to \nu_\tau$ and $\nu_e \to \nu_\tau$ oscillation, Phys. Lett. B **497**, 8 (2001).
[79] P. Vilain *et al.* (CHARM II Collaboration), Search for muon to electron-neutrino oscillations, Z. Phys. C **64**, 539 (1994).
[80] M. Antonello *et al.* (ICARUS Collaboration), Search for anomalies in the ν_e appearance from a ν_μ beam, Eur. Phys. J. C **73**, 2599 (2013).
[81] S. Avvakumov *et al.* (NuTeV Collaboration), A Search for $\nu_\mu \to \nu_e$ and $\bar{\nu}_\mu \to \bar{\nu}_e$ Oscillations at NuTeV, Phys. Rev. Lett. **89**, 011804 (2002).
[82] M. G. Aartsen *et al.* (IceCube Collaboration), A combined maximum-likelihood analysis of the high-energy astrophysical neutrino flux measured with IceCube, Astrophys. J. **809**, 98 (2015).
[83] J. Stachurska, IceCube upgrade and gen-2, https://indico.desy.de/indico/event/18204/session/14/contribution/221/material/slides/0.pdf.
[84] I. M. Shoemaker and K. Murase, Probing BSM neutrino physics with flavor and spectral distortions: Prospects for future high-energy neutrino telescopes, Phys. Rev. D **93**, 085004 (2016).
[85] M. G. Aartsen *et al.* (IceCube-Gen2 Collaboration), IceCube-Gen2: The window to the extreme Universe, J. Phys. G **48**, 060501 (2021).
[86] N. Song, S. W. Li, C. A. Argüelles, M. Bustamante, and A. C. Vincent, The future of high-energy astrophysical neutrino flavor measurements, J. Cosmol. Astropart. Phys. 04 (2021) 054.
[87] T. Kashti and E. Waxman, Flavoring Astrophysical Neutrinos: Flavor Ratios Depend on Energy, Phys. Rev. Lett. **95**, 181101 (2005).
[88] W. Winter, Describing the observed cosmic neutrinos by interactions of nuclei with matter, Phys. Rev. D **90**, 103003 (2014).
[89] Y. Sui and P. S. Bhupal Dev, A combined astrophysical and dark matter interpretation of the IceCube HESE and throughgoing muon events, J. Cosmol. Astropart. Phys. 07 (2018) 020.
[90] E. Waxman and J. N. Bahcall, High-Energy Neutrinos from Cosmological Gamma-Ray Burst Fireballs, Phys. Rev. Lett. **78**, 2292 (1997).
[91] J. P. Rachen and P. Meszaros, Photohadronic neutrinos from transients in astrophysical sources, Phys. Rev. D **58**, 123005 (1998).
[92] P. Lipari, M. Lusignoli, and D. Meloni, Flavor composition and energy spectrum of astrophysical neutrinos, Phys. Rev. D **75**, 123005 (2007).
[93] C. A. Argüelles, T. Katori, and J. Salvado, New Physics in Astrophysical Neutrino Flavor, Phys. Rev. Lett. **115**, 161303 (2015).
[94] M. Bustamante, J. F. Beacom, and W. Winter, Theoretically Palatable Flavor Combinations of Astrophysical Neutrinos, Phys. Rev. Lett. **115**, 161302 (2015).
[95] V. Brdar, J. Kopp, and X.-P. Wang, Sterile neutrinos and flavor ratios in IceCube, J. Cosmol. Astropart. Phys. 01 (2017) 026.
[96] M. Bustamante, A. M. Gago, and J. Jones Perez, SUSY renormalization group effects in ultra high energy neutrinos, J. High Energy Phys. 05 (2011) 133.
[97] R. Howarth, Sources for a history of the ternary diagram, Br. J. Hist. Sci. **29**, 337 (1996).
[98] J. G. Learned and S. Pakvasa, Detecting ν_τ oscillations at PeV energies, Astropart. Phys. **3**, 267 (1995).